

Passivity-based Control of VTOL UAVs with a Momentum-based Estimator of External Wrench and Unmodeled Dynamics

Fabio Ruggiero^{a,*}, Jonathan Cacace^a, Hamid Sadeghian^b, Vincenzo Lippiello^a

^a*PRISMA Lab, Department of Electrical Engineering and Information Technology, University of Naples, via Claudio 21, 80125, Naples, Italy.*

^b*Engineering Department, University of Isfahan, Isfahan 8174673441, Iran.*

Abstract

A passivity-based control of Vertical Take-off and Landing (VTOL) Unmanned Aerial Vehicles (UAVs) is presented in this paper. An estimator of unmodeled dynamics and external wrench (forces plus moments) acting on the aerial vehicle and based on the momentum of the system is employed to compensate such disturbances effects. This arrangement allows VTOL UAVs to perform hovering, tracking and aerial manipulation tasks in unstructured environments. A rigorous stability proof is provided under certain assumptions. Experiments are presented to evaluate the performance of the proposed control design.

Keywords: passivity-based control, external wrench estimation, unmodeled dynamics, VTOL UAV control

1. Introduction

Service robotics applications are day by day making more use of VTOL UAVs to pursue different actions. From passive tasks like inspection [1, 2], surveillance and monitoring [3], remote sensing and so on, such aerial vehicles are now beginning to be employed in active tasks like grasping [4] and manipulation [5, 6, 7, 8, 9, 10, 11, 12, 13, 14, 15, 16]. This change of perspective requires the UAV to operate in changing and unstructured scenarios. To this purpose, the controller has to deal with unknown parameters (i.e., the battery charge level), the transportation of unknown payloads, aerodynamic effects that are usually neglected during the control design phase, and the interaction with the environment.

In this paper, a passivity-based control of VTOL UAVs is presented. The classical hierarchical architecture separating the (fast) rotational and the (slow) translational dynamics [17] is employed. The controller ensures a closed-loop mechanical impedance behaviour for the translational part of the VTOL UAV, while the rotational part does not

rely upon exact cancellation of nonlinearities, conferring in this way robustness to the attitude part. The collision identification technique based on the momentum of the system proposed in [18] has been suitably modified in this context to play as an external wrench and unmodeled dynamics estimator. The estimation is taken into account by the controller to compensate forces and moments arising from wind, aerodynamics effects not taken into account in the model, external wrench caused by a robotic arm attached to the vehicle's base during aerial manipulation tasks, unknown carried payloads, physical interactions, and so on. The residual errors between the estimated external wrench, the unmodeled dynamics and the real ones are seen as perturbations in the closed-loop system. As long as the closed-loop system bandwidth –tunable through the control gains on the basis of the available robotic platform and the controller sample time– is able to cope with such time-varying residual errors, the overall performance benefits from the proposed architecture as theoretically and experimentally evaluated.

As far as authors know, the novelty of this paper is the combination of a passivity-based control for VTOL UAVs together with an external wrench and unmodeled dynamics estimator, a rigorous stability proof under certain assumptions, and the con-

*Corresponding author

Email address: fabio.ruggiero@unina.it (Fabio Ruggiero)

sequent experimental validation. As a result, the aerial platform is able to perform tasks without a precise knowledge about the dynamic parameters and the external disturbances: this is absolutely useful in the forthcoming aerial service robotics applications, e.g. aerial manipulation, where interaction with the environment is required. Moreover, with respect to the current state of the art in which adaptive and integral actions are employed to cope with the aforementioned problems, less parameters have to be tuned in the proposed architecture, where instead the gains assume precise physical meanings.

The outline of the paper is as follows. Next section presents the related work. The dynamic model of a quadrotor is presented in Section 3. The momentum-based external wrench and unmodeled dynamics estimator is revised in Section 4. The control is introduced in Section 5. The stability proof of the proposed controller combined with the compensation of the estimated terms is addressed in Section 6. Performed experiments are described in Section 7. Conclusion and future work are finally provided.

2. Related work

Regarding aerial manipulation, two approaches can be in principle thought to control an aerial manipulator (UAV with an attached robotic arm endowed with a gripper). The former approach considers the UAV and the robotic arm as a unique entity, and thus the controller is designed on the basis of such complete dynamic model [9, 10, 19]. The latter approach considers instead the UAV and the robotic arm as two separate and independent systems: the effects of the arm on the aerial vehicle are then considered as external disturbances and viceversa. This might be useful in case the dynamics of the arm is not enough to compensate the UAV position error and/or in case the arm does not allow torque control (i.e., servomotors) [20]. The here presented paper is oriented towards the latter approach: it has been thus considered the control of the single UAV subject to external disturbances and time-varying parameters. Therefore, many different approaches address problems related to the stabilization and tracking of desired trajectories with a VTOL UAV. The most widely used controller takes into account a hierarchical architecture [17, 21] highlighting a time-scale separation

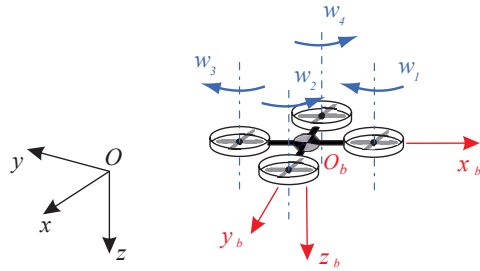


Figure 1: Quadrotor and related frames. In black, the inertial frame Σ_i . In red, the body frame Σ_b . In blue, the propellers speed and the label of each motor.

between the translational (slow time-scale) and angular (fast time-scale) dynamics of the aerial vehicle. Other approaches rely upon backstepping [22], impedance [23] and optical flow [24] techniques. However, in general, a precise knowledge of system dynamics is required to perform a feedback linearization of both fast and slow time-scale parts of the system. Hence, several of the above mentioned controllers implement an integral action to resist against external disturbances and cope with unknown and time varying parameters. Recently, adaptive controls have been employed to counteract such disturbances [14, 25, 26, 27, 28, 29]. A nonlinear force observer has been introduced in [30] to estimate disturbances applied to a quadrotor. A sliding mode observer has been instead employed in [31] to impose more robustness on the closed-loop system. Since passivity-based controllers do not rely on the exact compensation of the considered model, they are expected to be more robust with respect to parameters uncertainties. Port-Hamiltonian methods have been developed in [30, 32, 33], a passive backstepping in [34], and passivity-based attitude controls in [35, 36], in particular without angular velocity measurement in [37, 38].

In this paper, the passivity-based control proposed in [39, 40] is adapted to be suitable for a VTOL UAV system as described in Section 5. Moreover, a compensation of external wrench and unmodeled dynamics is here introduced to further reduce aerodynamic effects and external disturbances. A similar architecture has been introduced by the authors in [41] where an impedance controller is instead employed without providing a rigorous stability proof. Under certain assumptions, this issue is overcome by the current paper.

3. Modeling

The most popular configurations of VTOL UAVs employed in the above defined scenarios are the *quadrotor* and the *hexarotor*, which are platforms equipped with four or six propellers, respectively, aligned in the same direction. Hence, these aerial vehicles are underactuated mechanical systems having six degrees of freedom but only four independent control inputs. Without loss of generality, in the remainder of this paper, the chosen VTOL UAV is a quadrotor.

Define a world-fixed inertia reference frame Σ_i and a body-fixed reference frame Σ_b placed at the UAV's center of mass (see Fig. 1). The absolute position of the UAV with respect to Σ_i is denoted by $\mathbf{p}_b = [x \ y \ z]^T$. Using the roll-pitch-yaw Euler angles, $\boldsymbol{\eta}_b = [\phi \ \theta \ \psi]^T$, the attitude of the UAV is defined by the rotation matrix $\mathbf{R}_b(\boldsymbol{\eta}_b) \in \text{SO}(3)$, expressing the rotation of Σ_b with respect to Σ_i , given by [42]

$$\mathbf{R}_b(\boldsymbol{\eta}_b) = \begin{bmatrix} c_\theta c_\psi & s_\phi s_\theta c_\psi - c_\phi s_\psi & c_\phi s_\theta c_\psi + s_\phi s_\psi \\ c_\theta s_\psi & s_\phi s_\theta s_\psi + c_\phi c_\psi & c_\phi s_\theta s_\psi - s_\phi c_\psi \\ -s_\theta & s_\phi c_\theta & c_\phi c_\theta \end{bmatrix},$$

where s_\times and c_\times are abbreviations for sine and cosine, respectively.

Let $\dot{\mathbf{p}}_b$ and $\boldsymbol{\omega}_b$ denote the absolute translational and angular velocities of the UAV, respectively, while $\dot{\mathbf{p}}_b^b$ and $\boldsymbol{\omega}_b^b$ describe the absolute translational and angular velocities of the aerial vehicle expressed in Σ_b , respectively. Denoting with $\dot{\boldsymbol{\eta}}_b$ the time derivative of $\boldsymbol{\eta}_b$, the following equations hold [42]

$$\dot{\mathbf{p}}_b = \mathbf{R}_b(\boldsymbol{\eta}_b) \dot{\mathbf{p}}_b^b, \quad (1a)$$

$$\boldsymbol{\omega}_b = \mathbf{T}_b(\boldsymbol{\eta}_b) \dot{\boldsymbol{\eta}}_b, \quad (1b)$$

$$\boldsymbol{\omega}_b^b = \mathbf{R}_b(\boldsymbol{\eta}_b)^T \boldsymbol{\omega}_b = \mathbf{Q}(\boldsymbol{\eta}_b) \dot{\boldsymbol{\eta}}_b, \quad (1c)$$

where $\mathbf{T}_b(\boldsymbol{\eta}_b)$ is the (3×3) transformation matrix between the time derivative of $\boldsymbol{\eta}_b$ and the correspondent $\boldsymbol{\omega}_b$, while $\mathbf{Q}(\boldsymbol{\eta}_b) = \mathbf{R}_b(\boldsymbol{\eta}_b)^T \mathbf{T}_b(\boldsymbol{\eta}_b)$ maps the time derivative of $\boldsymbol{\eta}_b$ into the UAV angular velocity expressed with respect to Σ_b . The detailed expression of $\mathbf{Q}(\boldsymbol{\eta}_b)$ is

$$\mathbf{Q}(\boldsymbol{\eta}_b) = \begin{bmatrix} 1 & 0 & -s_\theta \\ 0 & c_\phi & c_\theta s_\phi \\ 0 & -s_\phi & c_\theta c_\phi \end{bmatrix},$$

with a singularity at $\theta = \pm\pi/2$.

The dynamic equations related to the UAV can be retrieved by using the Newton-Euler formulation [43]

$$m\ddot{\mathbf{p}}_b^b = -m\mathbf{S}(\boldsymbol{\omega}_b^b)\dot{\mathbf{p}}_b^b + m\mathbf{R}_b(\boldsymbol{\eta}_b)^T \mathbf{g} + \mathbf{f}_b^b + \mathbf{f}_u^b(\cdot), \quad (2a)$$

$$\dot{\mathbf{R}}_b(\boldsymbol{\eta}_b) = \mathbf{R}_b(\boldsymbol{\eta}_b) \mathbf{S}(\boldsymbol{\omega}_b) \quad (2b)$$

$$\mathbf{I}_b \dot{\boldsymbol{\omega}}_b^b = -\mathbf{S}(\boldsymbol{\omega}_b^b) \mathbf{I}_b \boldsymbol{\omega}_b^b + \boldsymbol{\tau}_b^b + \boldsymbol{\tau}_u^b(\cdot), \quad (2c)$$

where $\ddot{\mathbf{p}}_b^b$ is the absolute translational acceleration of the UAV expressed with respect to Σ_b ; m is the mass of the vehicle; \mathbf{I}_b is the (3×3) constant inertia matrix of the UAV expressed with respect to Σ_b ; $\dot{\boldsymbol{\omega}}_b^b$ is the absolute angular acceleration of the UAV expressed with respect to Σ_b ; $\mathbf{S}(\cdot)$ denotes the skew-symmetric matrix; $\mathbf{g} = [0 \ 0 \ g]^T$ is the (3×1) gravity vector with $g = 9.81\text{m/s}^2$; \mathbf{f}_b^b and $\boldsymbol{\tau}_b^b$ are the (3×1) forces and torques input vectors, respectively, expressed in Σ_b ; $\mathbf{f}_u^b(\cdot)$ and $\boldsymbol{\tau}_u^b(\cdot)$ are two (3×1) vectors denoting unknown forces and moments, respectively, acting on the vehicle – aerodynamic and buoyancy effects, flapping dynamics [44], parametric uncertainties, imbalances caused by batteries and/or on-board sensors, motion of a robotic arm (or moving sensors, e.g. a laser scanner on a pan-tilt mechanism) mounted on the aerial platform, wind gusts, interaction with the environment, etc. – and whose dependencies on $(\dot{\mathbf{p}}_b, \ddot{\mathbf{p}}_b, \boldsymbol{\omega}_b^b, \dot{\boldsymbol{\omega}}_b^b, \mathbf{R}_b(\boldsymbol{\eta}_b), t)$, where t denotes the time variable, have been omitted for brevity.

The detailed expressions of both the input forces \mathbf{f}_b^b and torques $\boldsymbol{\tau}_b^b$ depend on the configuration of the considered aerial vehicle. Most of the VTOL UAVs are underactuated systems with six degrees of freedom and four main control inputs. Hence, many UAVs can be characterized by three input control torques $\boldsymbol{\tau}_b^b = [\tau_\phi \ \tau_\theta \ \tau_\psi]^T$ and one input control force $\mathbf{f}_b^b = [0 \ 0 \ u]^T$, where u denotes the thrust perpendicular to the propellers rotation plane. In the quadrotor case of Fig. 1, the relationship between the thrust, the control torques, and the squared propellers speed w_i^2 , with $i = 1, \dots, 4$, is [22]

$$u = \rho_u (w_1^2 + w_2^2 + w_3^2 + w_4^2), \quad (3a)$$

$$\tau_\phi = l\rho_u (w_2^2 - w_4^2), \quad (3b)$$

$$\tau_\theta = l\rho_u (w_3^2 - w_1^2), \quad (3c)$$

$$\tau_\psi = cw_1^2 - cw_2^2 + cw_3^2 - cw_4^2, \quad (3d)$$

where l is the distance between each propeller and the center of mass of the quadrotor, $\rho_u > 0$ and

$c > 0$ are the thrust and drag factors, respectively. It is worth noticing that many aerodynamics effects are neglected through this representation. However, in case of hovering, or at least low-speed motions, the relationships in (3) can be considered as a valid approximation [17].

Folding (1) and the relative time derivatives into (2), and considering the expression of \mathbf{f}_b^b yield the following dynamic model, useful for control design purposes, expressed with respect to Σ_i , and representing a wide range of VTOL UAVs configurations:

$$m\ddot{\mathbf{p}}_b = m\mathbf{g} - u\mathbf{R}_b(\boldsymbol{\eta}_b)\mathbf{i}_3 + \mathbf{f}_u(\cdot), \quad (4a)$$

$$\mathbf{M}(\boldsymbol{\eta}_b)\ddot{\boldsymbol{\eta}}_b = -\mathbf{C}(\boldsymbol{\eta}_b, \dot{\boldsymbol{\eta}}_b)\dot{\boldsymbol{\eta}}_b + \mathbf{Q}(\boldsymbol{\eta}_b)^T\boldsymbol{\tau}_b^b + \boldsymbol{\tau}_u(\cdot), \quad (4b)$$

where $\mathbf{i}_3 = [0 \ 0 \ 1]^T$; $\mathbf{M}(\boldsymbol{\eta}_b) = \mathbf{Q}(\boldsymbol{\eta}_b)^T\mathbf{I}_b\mathbf{Q}(\boldsymbol{\eta}_b)$ is the (3×3) symmetric and positive definite inertia matrix (provided that $\theta \neq \pm\pi/2$), and $\mathbf{C}(\boldsymbol{\eta}_b, \dot{\boldsymbol{\eta}}_b) = \mathbf{Q}^T\mathbf{S}(\mathbf{Q}\dot{\boldsymbol{\eta}}_b)\mathbf{I}_b\mathbf{Q} + \mathbf{Q}^T\mathbf{I}_b\dot{\mathbf{Q}}$ is the (3×3) Coriolis matrix, in which the dependencies have been dropped and $\dot{\mathbf{Q}}(\boldsymbol{\eta}_b)$ represents the time derivative of $\mathbf{Q}(\boldsymbol{\eta}_b)$.

Mentioning that only Euclidean norms are taken into account in the remainder of the paper, the following assumptions are considered.

- **Assumption 1.** The aerial vehicle does not pass through the singularities. The allowable configuration space for the yaw-pitch-roll angles $\boldsymbol{\eta}_b$ is thus $\mathcal{Q}_\eta = \{\boldsymbol{\eta}_b \in \mathbb{R}^3 | \theta \neq \pi/2 + k\pi, k = \dots, -1, 0, 1, \dots\}$.
- **Assumption 2.** Unknown forces $\mathbf{f}_u(\cdot)$ and moments $\boldsymbol{\tau}_u(\cdot)$ depend only on the time variable t and they are continuously differentiable and bounded with respect to it. Therefore, the following inequalities hold

$$\|\mathbf{f}_u\| \leq B_1 < \infty, \quad (5a)$$

$$\|\dot{\mathbf{f}}_u\| \leq B_2 < \infty, \quad (5b)$$

$$\|\ddot{\mathbf{f}}_u\| \leq B_3 < \infty, \quad (5c)$$

$$\|\boldsymbol{\tau}_u\| \leq B_4 < \infty, \quad (5d)$$

$$\|\dot{\boldsymbol{\tau}}_u\| \leq B_5 < \infty, \quad (5e)$$

$$\|\ddot{\boldsymbol{\tau}}_u\| \leq B_6 < \infty, \quad (5f)$$

where B_i , with $i = 1, \dots, 6$, are positive constants.

It is also worth to recall the following property.

- **Property 1.** Considering the expression in (4b), the following property holds [42]

$$\dot{\boldsymbol{\eta}}_b^T \left(\dot{\mathbf{M}}(\boldsymbol{\eta}_b) - 2\mathbf{C}(\boldsymbol{\eta}_b, \dot{\boldsymbol{\eta}}_b) \right) \dot{\boldsymbol{\eta}}_b = 0, \quad (6)$$

where $\dot{\mathbf{M}}(\boldsymbol{\eta}_b)$ represents the time derivative of $\mathbf{M}(\boldsymbol{\eta}_b)$. If the Coriolis matrix is represented through the Christoffel symbols, then for any arbitrary (3×1) vector \mathbf{v} the following quadratic form holds

$$\dot{\mathbf{v}}^T \left(\dot{\mathbf{M}}(\boldsymbol{\eta}_b) - 2\mathbf{C}(\boldsymbol{\eta}_b, \dot{\boldsymbol{\eta}}_b) \right) \dot{\mathbf{v}} = 0.$$

3.1. Discussion about the employed assumptions

The impact of the employed assumptions, made to simplify the control design, is deeply analysed in the following.

Assumption 1 is restrictive only from a mathematical point of view. The singularity about the pitch angle is related to the employed angular representation and it is not a physical singularity; moreover, notice that a pitch angle of $\pm\pi/2$ does not happen because acrobatic manoeuvres (i.e., death loops) are not within the goals of this work, the initial conditions are chosen far from that singularity condition and the controller will be shown to be stable. In addition, since only two points in the configuration space are not allowed, this case might also be handled from a practical point of view during the implementation of the programming code. It goes without saying that a non minimal representation for the rotations might be in principle employed, i.e. unit quaternions [45, 46, 47]. The related control laws guarantee almost global asymptotic stability¹. In any case, both Euler angles and quaternions representations suffer of the so-called *unwinding phenomenon* [48] if the control laws are not properly designed. In this paper, through the use of Assumption 1, the problem is related to the yaw angle². Nevertheless, the concept about the hybrid-dynamic path-lifting algorithm proposed in [48] can be easily implemented as a solution for both Euler angles and quaternions representations.

¹In the unit quaternion case, the problem is that, roughly speaking, different quaternions may represent the same physical attitude of the related rigid body [47].

²As an example, defining the yaw angle between $[0, 2\pi]$ and stabilizing the yaw around 0, it may happen that for some values of the yaw around 0 the controller tries to make an undesired complete rotation of the aerial vehicle.

With reference to Assumption 2, notice that the motivations about neglecting the dependence of the unknown forces and moments from the aerial vehicle's angular attitude, angular velocity and translational accelerations are taken from [43]. The independence of \mathbf{f}_u and $\boldsymbol{\tau}_u$ from $\dot{\mathbf{p}}_b$ and $\dot{\boldsymbol{\omega}}_b^b$ can be justified since, in general, the density of the body of the aerial platform is much more relevant than the one of the environment fluid. The independence from $\boldsymbol{\omega}_b^b$ is better justified when the unknown generalized forces apply near the aerial vehicle's center of mass and the motion reaction forces resulting from the rotation of the aerial platform can be neglected with respect to the ones produced by eventual linear movements. The independence from $\dot{\mathbf{p}}_b$ is the most restrictive one since it is supposed that the aerial vehicle moves very slowly and for almost all the task it is in hovering. Such an assumption is much more justified in aerial manipulation tasks. However, on the one hand, such condition simplifies the derivation of the control law and its stability proof; on the other hand, during experimental validation in Section 7, the hovering condition is overcome and the performance of the control law is evaluated despite the employed assumption. The independence from the vehicle's attitude $\mathbf{R}_b(\boldsymbol{\eta}_b)$ is valid when the aerodynamic forces do not depend on the aerial platform orientation. This happens essentially on the basis of the vehicle's shape. In case of VTOL UAVs such assumption is thus very reasonable due to the fact that lift forces are not so sensitive with respect to the attack angles. In conclusion, thanks to Assumption 2, the unknown forces and moments are only time depending and their boundedness is not so much restrictive, but instead properly physically justified as underlined in [43].

4. Momentum-based estimator of external wrench and unmodeled dynamics

The (6×1) generalized momentum vector of the system (4) can be defined as

$$\mathbf{q} = \begin{bmatrix} m\mathbf{I}_3 & \mathbf{O}_3 \\ \mathbf{O}_3 & \mathbf{M}(\boldsymbol{\eta}_b) \end{bmatrix} \begin{bmatrix} \dot{\mathbf{p}}_b \\ \dot{\boldsymbol{\eta}}_b \end{bmatrix}, \quad (7)$$

where \mathbf{I}_n and \mathbf{O}_n are $(n \times n)$ identity and zero matrices, respectively. From the expressions of $\mathbf{M}(\boldsymbol{\eta}_b)$ and $\mathbf{C}(\boldsymbol{\eta}_b, \dot{\boldsymbol{\eta}}_b)$ and from Property 1, it is possible to prove that the following expression holds

$$\dot{\mathbf{M}}(\boldsymbol{\eta}_b, \dot{\boldsymbol{\eta}}_b) = \mathbf{C}(\boldsymbol{\eta}_b, \dot{\boldsymbol{\eta}}_b) + \mathbf{C}(\boldsymbol{\eta}_b, \dot{\boldsymbol{\eta}}_b)^T. \quad (8)$$

By using (4) and (8), the time derivative of the generalized momentum vector (7) is

$$\dot{\mathbf{q}} = \begin{bmatrix} -u\mathbf{R}_b(\boldsymbol{\eta}_b)\mathbf{i}_3 + \mathbf{f}_u(t) + m\mathbf{g} \\ \mathbf{Q}(\boldsymbol{\eta}_b)^T\boldsymbol{\tau}_b^b + \boldsymbol{\tau}_u(t) + \mathbf{C}(\boldsymbol{\eta}_b, \dot{\boldsymbol{\eta}}_b)^T\dot{\boldsymbol{\eta}}_b \end{bmatrix}. \quad (9)$$

The goal of the proposed estimator is to achieve a linear relationship between the dynamics of the estimated external wrench, unmodeled effects and the real ones. Hence, in the Laplace's domain, such relationship has the following expression

$$\begin{bmatrix} \widehat{\mathbf{f}}_u(s) \\ \widehat{\boldsymbol{\tau}}_u(s) \end{bmatrix} = \mathbf{G}(s) \begin{bmatrix} \mathbf{f}_u(s) \\ \boldsymbol{\tau}_u(s) \end{bmatrix}, \quad (10)$$

where s is the complex variable in the Laplace's domain, $\widehat{\mathbf{f}}_u$ and $\widehat{\boldsymbol{\tau}}_u$ are the (3×1) vectors of the estimated unknown forces and moments, respectively, while $\mathbf{G}(s)$ is a (6×6) diagonal matrix of transfer functions in which the i -th element, with $i = 1, \dots, 6$, has the following expression

$$G_i(s) = \frac{\omega_{n,i}^2}{s^2 + 2\zeta_i\omega_{n,i}s + \omega_{n,i}^2}, \quad (11)$$

where $\omega_{n,i}$ and ζ_i are the desired natural frequency and damping of the designed estimator, respectively, for the i -th component.

In order to get (11) component-wise in (10), the expression of the estimated external wrench and unmodeled dynamics $\mathbf{r}(t) = \begin{bmatrix} \widehat{\mathbf{f}}_u^T & \widehat{\boldsymbol{\tau}}_u^T \end{bmatrix}^T$ in the time domain is defined as follows

$$\mathbf{r}(t) = \mathbf{K}_1 \left(\int_0^t -\mathbf{r}(\sigma) + \mathbf{K}_2 \left(\mathbf{q}(\sigma) - \int_0^t \left(\mathbf{r}(\sigma) + \begin{bmatrix} -u\mathbf{R}_b(\boldsymbol{\eta}_b)\mathbf{i}_3 + m\mathbf{g} \\ \mathbf{Q}(\boldsymbol{\eta}_b)^T\boldsymbol{\tau}_b^b + \mathbf{C}(\boldsymbol{\eta}_b, \dot{\boldsymbol{\eta}}_b)^T\dot{\boldsymbol{\eta}}_b \end{bmatrix} \right) d\sigma \right) d\sigma \right), \quad (12)$$

where it is assumed that ³ $\mathbf{q}(0) = \mathbf{r}(0) = \dot{\mathbf{r}}(0) = 0$, while $\mathbf{K}_1 = \text{diag}\{\mathbf{K}_{1,1}, \mathbf{K}_{1,2}\}$ and $\mathbf{K}_2 = \text{diag}\{\mathbf{K}_{2,1}, \mathbf{K}_{2,2}\}$ are (6×6) positive definite diagonal matrices, in which $\mathbf{K}_{i,j}$, $i, j = \{1, 2\}$, is a (3×3) positive definite diagonal matrix. Considering (4) and (9), the dynamics of (12) is

$$\ddot{\mathbf{r}} + \mathbf{K}_1\dot{\mathbf{r}} + \mathbf{K}_1\mathbf{K}_2\mathbf{r} = \mathbf{K}_1\mathbf{K}_2 \begin{bmatrix} \mathbf{f}_u \\ \boldsymbol{\tau}_u \end{bmatrix}, \quad (13)$$

that in Laplace domain is equivalent to the 6 transfer functions in (10). Once the natural frequencies

³This condition means that, in the practice, the estimator has to start before the take-off of the UAV.

and the damping factors in (11) have been designed, the components of the gains \mathbf{K}_1 and \mathbf{K}_2 in (12) can be computed as follows

$$\begin{aligned} k_{1,i}k_{2,i} &= \omega_{n,i}^2 \\ k_{1,i} &= 2\zeta_i\omega_{n,i} \end{aligned}$$

where $i = 1, \dots, 6$, and $k_{1,i}$ and $k_{2,i}$ are the i -th elements of \mathbf{K}_1 and \mathbf{K}_2 , respectively.

Notice that, in ideal case,

$$\zeta_i \rightarrow 1 \quad \omega_{n,i} \rightarrow \infty \implies \mathbf{r}(t) = \begin{bmatrix} \hat{\mathbf{f}}_u \\ \hat{\boldsymbol{\tau}}_u \end{bmatrix} \approx \begin{bmatrix} \mathbf{f}_u \\ \boldsymbol{\tau}_u \end{bmatrix},$$

where $i = 1, \dots, 6$, which means that the gains should be taken as large as possible in the practice.

The quantities required to compute \mathbf{r} are the UAV orientation $\boldsymbol{\eta}_b$ and the related time derivative $\dot{\boldsymbol{\eta}}_b$, the vehicle translational velocity $\dot{\mathbf{p}}_b$, the commanded input torques $\boldsymbol{\tau}_b^b$, the thrust u and the knowledge about the UAV inertia matrix \mathbf{I}_b and mass m . The quantities $\boldsymbol{\eta}_b$ and $\dot{\boldsymbol{\eta}}_b$ can be retrieved by the on-board IMU sensor, while $\dot{\mathbf{p}}_b$ can be estimated by using GPS and/or visual data [49, 50]. The thrust u and the input torques $\boldsymbol{\tau}_b^b$ are given by the passivity-based controller (see Section 5). The UAV inertia \mathbf{I}_b and mass m should be instead known a-priori. Notice that no inversion of the inertia matrix $\mathbf{M}(\boldsymbol{\eta}_b)$ is required, and also no knowledge about the absolute position \mathbf{p}_b of the UAV is needed. Moreover, notice that, with respect to [18], a second-order transfer function has been considered to better weaken the effects of high-frequencies noise (e.g., introduced by both the IMU sensor and the estimation of $\dot{\mathbf{p}}_b$) that overcomes the selected bandwidth designed through the choice of $\boldsymbol{w}_{n,i}$, with $i = 1, \dots, 3$. Notice that with small modifications to (12), it is possible to reach a transfer function in (10) of the desired order.

5. VTOL UAVs passivity-based control

The time scale separation highlighted in the classical hierarchical controllers [17, 21] is traduced in a inner-outer loop control architecture. Namely, the inner loop is devoted to control the fast time-scale angular part, while the outer loop tackles the slow time-scale position tracking part. Because of the underactuation of the system, only 4 components can be provided by an external planner. Since \mathbf{p}_b and ψ are flat outputs for the system (4) [51], the planner gives as inputs to the controller the desired position trajectory of the UAV, described by

the (3×1) vectors \mathbf{p}_d , $\dot{\mathbf{p}}_d$ and $\ddot{\mathbf{p}}_d$, and the desired yaw trajectory, described by ψ_d , $\dot{\psi}_d$ and $\ddot{\psi}_d$. Hence, the desired pitch and roll components are implicitly computed on the basis of the planned UAV position and yaw.

For the inner loop, let $\boldsymbol{\eta}_d = [\phi_d \ \theta_d \ \psi_d]^T$ be the (3×1) vector of the UAV desired attitude with $\dot{\boldsymbol{\eta}}_d$ and $\ddot{\boldsymbol{\eta}}_d$ its time derivatives. Define the following (3×1) reference vector for the attitude velocity

$$\dot{\boldsymbol{\eta}}_r = \dot{\boldsymbol{\eta}}_d - \nu \mathbf{e}_\eta, \quad (14)$$

where $\mathbf{e}_\eta = \boldsymbol{\eta}_b - \boldsymbol{\eta}_d$ is the (3×1) angular tracking error and $\nu > 0$ a coupling parameter. The following passivity-based control input can be then defined for the inner loop

$$\begin{aligned} \boldsymbol{\tau}_b^b &= \mathbf{Q}(\boldsymbol{\eta}_b)^{-T} (\mathbf{M}(\boldsymbol{\eta}_b)\ddot{\boldsymbol{\eta}}_r + \mathbf{C}(\boldsymbol{\eta}_b, \dot{\boldsymbol{\eta}}_b)\dot{\boldsymbol{\eta}}_r - \hat{\boldsymbol{\tau}}_u \\ &\quad - \mathbf{D}_o \mathbf{v}_\eta - \mathbf{K}_o \mathbf{e}_\eta), \end{aligned} \quad (15)$$

where \mathbf{D}_o and \mathbf{K}_o are (3×3) positive definite diagonal gain matrices, $\dot{\mathbf{e}}_\eta = \dot{\boldsymbol{\eta}}_b - \dot{\boldsymbol{\eta}}_d$, $\ddot{\boldsymbol{\eta}}_r = \ddot{\boldsymbol{\eta}}_d - \nu \dot{\mathbf{e}}_\eta$ and $\mathbf{v}_\eta = \dot{\mathbf{e}}_\eta + \nu \mathbf{e}_\eta$. Considering (4b), notice that no cancellation of dynamic model terms is performed through (15).

The outer loop has then to provide the desired thrust and the reference values of the pitch and roll angles. Define a (3×1) virtual input acceleration vector $\boldsymbol{\mu}$ devoted to the position tracking part and that will be designed in the following. It should be possible to retrieve the thrust and the desired attitude angles values for the inner loop from the virtual control input $\boldsymbol{\mu}$. For this reason, it is imposed that

$$\boldsymbol{\mu} = -\frac{u}{m} \mathbf{R}_b(\boldsymbol{\eta}_d) \mathbf{i}_3 + \mathbf{g} + \frac{1}{m} \hat{\mathbf{f}}_u, \quad (16)$$

representing the desired acceleration vector with respect to Σ_i , in which the magnitude is the thrust u produced by the propellers, while the orientation is given by the desired UAV attitude. Properly designing $\boldsymbol{\mu}$, inverting (16) it is then possible to retrieve the desired values for the thrust and the attitude angles that are in turn exploited as references for the inner control loop. Therefore, let $\mathbf{e}_p = \mathbf{p}_b - \mathbf{p}_d$, $\dot{\mathbf{e}}_p = \dot{\mathbf{p}}_b - \dot{\mathbf{p}}_d$, $\ddot{\mathbf{e}}_p = \ddot{\mathbf{p}}_b - \ddot{\mathbf{p}}_d$ and $\ddot{\mathbf{e}}_\eta = \ddot{\boldsymbol{\eta}}_b - \ddot{\boldsymbol{\eta}}_d$ be the (3×1) tracking errors, and let $\tilde{\mathbf{f}} = \mathbf{f}_u - \hat{\mathbf{f}}_u$ be the estimated force error. Replacing both $\boldsymbol{\eta}_b = \boldsymbol{\eta}_d + \mathbf{e}_\eta$ and $\mathbf{f}_u = \hat{\mathbf{f}}_u + \tilde{\mathbf{f}}$ in (4a), recalling (16), yields

$$\ddot{\mathbf{p}}_b = \boldsymbol{\mu} + \frac{u}{m} \boldsymbol{\delta}(\boldsymbol{\eta}_d, \mathbf{e}_\eta) + \frac{1}{m} \tilde{\mathbf{f}}, \quad (17)$$

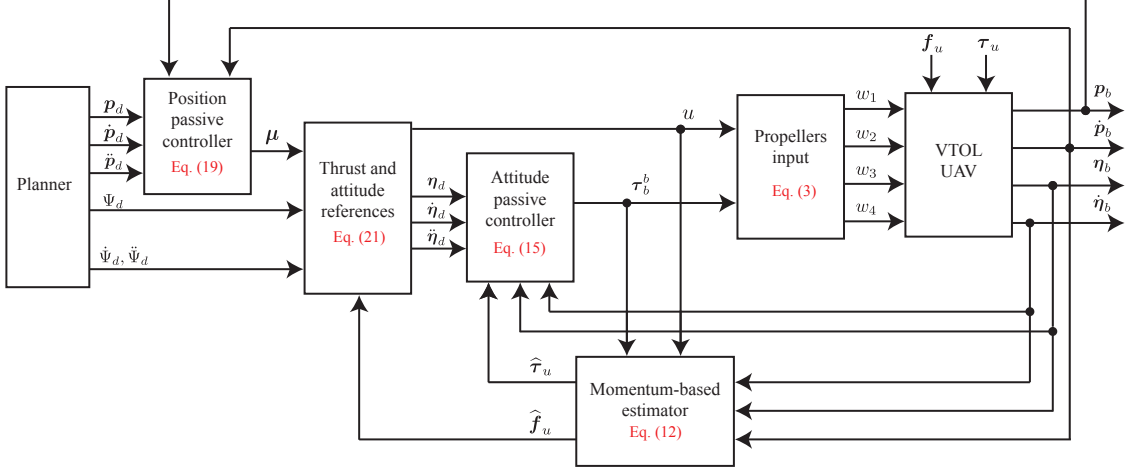


Figure 2: Block scheme of the proposed control architecture. In red, the corresponding equations in the paper related to each block.

where $\delta(\eta_d, e_\eta) = [\delta_x \ \delta_y \ \delta_z]^T$ is the following (3×1) interconnection vector

$$\delta = \begin{bmatrix} s_{\phi_d} s_{\psi_d} - s_\phi s_\psi - c_\phi c_\psi s_\theta + c_{\phi_d} c_{\psi_d} s_{\theta_d} \\ c_\psi s_\phi - c_{\psi_d} s_{\phi_d} + c_{\phi_d} s_{\theta_d} s_{\psi_d} - c_\phi s_\theta s_\psi \\ c_{\theta_d} c_{\phi_d} - c_\theta c_\phi \end{bmatrix}, \quad (18)$$

with $\phi = e_\phi + \phi_d$, $\theta = e_\theta + \theta_d$ and $\psi = e_\psi + \psi_d$. The virtual control input μ can now be chosen as

$$\mu = \ddot{p}_d - \frac{1}{m} (D_p \dot{e}_p + K_p e_p), \quad (19)$$

where D_p and K_p are two (3×3) positive definite diagonal gain matrices.

Folding (15) and (19) into (4b) and (17), respectively, yields the following closed-loop equations

$$m\ddot{e}_p + D_p \dot{e}_p + K_p e_p = u\delta(\eta_d, e_\eta) + \tilde{f}, \quad (20a)$$

$$M(\eta_b)\dot{v}_\eta + (C(\eta_b, \dot{\eta}_b) + D_o)v_\eta + K_o e_\eta = \tilde{\tau}, \quad (20b)$$

where $\dot{v}_\eta = \ddot{e}_\eta + \nu \dot{e}_\eta$ and $\tilde{\tau} = \tau_u - \hat{\tau}_u$. The right side of equation (20a) acts like an external force on the first subsystem and depends on both the UAV attitude error and the estimated unknown forces error. The right side of equation (20b) is the residual of the estimated moments and acts as a disturbance on the second subsystem. Thus, the expressions in (20) establish passive relationships between the reconstruction errors of generic unknown disturbances and the tracking errors. In particular, for equation (20b), as underlined in [52], there exists a passive mapping between $\tilde{\tau}$ and v_η , at least in hovering case.

- **Remark 1.** Notice that the relationship in (20a) is equivalent to a generalized mechanical impedance reacting to the external disturbance given by $(u\delta(\eta_d, e_\eta) + \tilde{f})$ with the same mass m of the aerial vehicle, and with a stiffness and damping that are programmable through the choice of the gain matrices K_p and D_p , respectively.

- **Remark 2.** The gains that have to be tuned in the proposed controller are namely: K_1 and K_2 for the estimator; K_p and D_p for the UAV translational part; ν , K_o and D_o for the angular one. A discussion about how to choose ν is done in [53], while the physical meanings of K_p and D_p are given in Remark 1. K_o and D_o might have similar meanings of programmable stiffness and damping of a torsional spring. The translational part is the slowest one due to the time-scale separation and because it depends on the attitude error. Hence, once the desired stiffness K_p and damping D_p have been chosen, it is possible to retrieve the closed-loop bandwidth of the controlled system. Then, the natural frequency and damping factor of the estimator can be tuned on the basis of this choice. In particular, they have to be at least larger than those designed for the UAV translational part so as not to weaken the closed-loop designed performance.

To recap, the proposed architecture is depicted in the block scheme of Fig. 2. After computing the position tracking errors e_p and \dot{e}_p , and knowing

the feedforward acceleration $\ddot{\mathbf{p}}_d$, the virtual control input $\boldsymbol{\mu}$ can be computed as in (19). The desired thrust u and the reference pitch and roll can be computed by inverting (16) as follows [17]

$$u = m\sqrt{\bar{\mu}_1^2 + \bar{\mu}_2^2 + (\bar{\mu}_3 - g)^2}, \quad (21a)$$

$$\phi_d = \sin^{-1}\left(m\frac{\bar{\mu}_2 \cos \psi_d - \bar{\mu}_1 \sin \psi_d}{u}\right), \quad (21b)$$

$$\theta_d = \text{atan2}(\bar{\mu}_1 \cos \psi_d + \bar{\mu}_2 \sin \psi_d, \bar{\mu}_3 - g), \quad (21c)$$

where $\bar{\boldsymbol{\mu}} = [\bar{\mu}_1 \ \bar{\mu}_2 \ \bar{\mu}_3]^\top = \boldsymbol{\mu} - (1/m)\hat{\mathbf{f}}_u$, with $\hat{\mathbf{f}}_u$ given by (12), while the desired yaw ψ_d is given by the planner. A second-order low-pass digital filter should be employed to reduce noise and compute both first and second derivatives of $\boldsymbol{\eta}_d$ [17], so as to get $\dot{\boldsymbol{\eta}}_d$ and $\ddot{\boldsymbol{\eta}}_d$, and hence compute in turn the attitude tracking errors \mathbf{e}_η and $\dot{\mathbf{e}}_\eta$. The control input vector $\boldsymbol{\tau}_b^b$ is computed as in (15), in which $\hat{\boldsymbol{\tau}}_u$ is given by (12). Having both the thrust u and the actuation torques $\boldsymbol{\tau}_b^b$, the squared propellers speeds w_i^2 of the VTOL UAV, with $i = 1, \dots, 4$, are computed by inverting (3).

• **Remark 3.** Notice that in case $\bar{\boldsymbol{\mu}} = \boldsymbol{\mu} - (1/m)\hat{\mathbf{f}}_u = \mathbf{g}$, equation (21b) is indeterminate. This exact condition is very difficult to happen in the practice but it can not be a priori excluded. From a physical point of view, such numeric singularity means a desired acceleration for the UAV equal to the gravity: this can be achieved with a zero thrust, i.e. turning off the propellers as it is evident from (3a). When the propellers are turned off, any values for the pitch and the roll are not reachable since the control is obviously not in action. In the practice, such a particular and uncommon condition can be nonetheless easily managed from a software point of view once the thrust is calculated as in (21a). It is worth remarking that no problems happened during the experiments, some of which are described in Section 7.

• **Remark 4.** Although it is of less interest, the passivity-based approach here proposed can be employed also without considering the compensation of external wrench and unmodeled dynamics, i.e. neglecting the term $\hat{\boldsymbol{\tau}}_u$ in (15) and with $\bar{\boldsymbol{\mu}} = \boldsymbol{\mu}$ in (21). As highlighted in [54], the use of integral/adaptive actions, as well as of external disturbances observers, might in some cases worsen and not improve

the controller performance. Therefore, in the reminder of the paper and during the experiments, it will be checked under which conditions the compensation of the estimated terms improves the performance of the sole passivity-based controller.

6. Stability proof

This section is devoted to show the stability of the whole control scheme made up by the momentum-based estimator of external wrench and unmodeled dynamics, and the passivity-based controller. It is worth mentioning that only marginal stability can be ensured since perturbation terms on the right sides of (20) might be nonvanishing. Moreover, it is also shown how adding the compensation of the estimated terms may help in reducing the asymptotic bounds of the closed-loop systems.

Let $\mathbf{x}_1 = [\mathbf{e}_p^\top \ \dot{\mathbf{e}}_p^\top]^\top$ and $\mathbf{x}_2 = [\mathbf{e}_\eta^\top \ \dot{\mathbf{e}}_\eta^\top]^\top$ be two (6×1) vectors denoting the state of the closed-loop system equations (20a) and (20b), respectively, which can also be arranged in the following way

$$\dot{\mathbf{x}}_1 = \boldsymbol{\alpha}_1(m, \mathbf{x}_1, \mathbf{K}_p, \mathbf{D}_p) + \boldsymbol{\beta}_1(u, m, \boldsymbol{\eta}_d, \mathbf{e}_\eta, \tilde{\mathbf{f}}), \quad (22a)$$

$$\dot{\mathbf{x}}_2 = \boldsymbol{\alpha}_2(\nu, \mathbf{x}_2, \boldsymbol{\eta}_b, \dot{\boldsymbol{\eta}}_b, \mathbf{K}_o, \mathbf{D}_o) + \boldsymbol{\beta}_2(\boldsymbol{\eta}_b, \tilde{\boldsymbol{\tau}}), \quad (22b)$$

where

$$\begin{aligned} \boldsymbol{\alpha}_1 &= \begin{bmatrix} \dot{\mathbf{e}}_p \\ -(1/m)\mathbf{D}_p\dot{\mathbf{e}}_p - (1/m)\mathbf{K}_p\mathbf{e}_p \end{bmatrix}, \\ \boldsymbol{\alpha}_2 &= \begin{bmatrix} \dot{\mathbf{e}}_\eta \\ -\mathbf{M}^{-1}(\nu\dot{\mathbf{e}}_\eta + (\mathbf{C} + \mathbf{D}_o)\mathbf{v}_\eta + \mathbf{K}_o\mathbf{e}_\eta) \end{bmatrix}, \\ \boldsymbol{\beta}_1 &= \begin{bmatrix} \mathbf{0}_3 \\ (u/m)\boldsymbol{\delta} + (1/m)\tilde{\mathbf{f}} \end{bmatrix}, \\ \boldsymbol{\beta}_2 &= \begin{bmatrix} \mathbf{0}_3 \\ \mathbf{M}^{-1}\tilde{\boldsymbol{\tau}} \end{bmatrix}, \end{aligned}$$

in which dependences have been dropped and $\mathbf{0}_n$ is the $(n \times 1)$ null vector. Let define the *nominal* systems as the closed-loop equations (22) without the perturbation terms $\boldsymbol{\beta}_1(u, m, \boldsymbol{\eta}_d, \mathbf{e}_\eta, \tilde{\mathbf{f}})$ and $\boldsymbol{\beta}_2(\boldsymbol{\eta}_b, \tilde{\boldsymbol{\tau}})$

$$\dot{\mathbf{x}}_1 = \boldsymbol{\alpha}_1(m, \mathbf{x}_1, \mathbf{K}_p, \mathbf{D}_p), \quad (23a)$$

$$\dot{\mathbf{x}}_2 = \boldsymbol{\alpha}_2(\nu, \mathbf{x}_2, \boldsymbol{\eta}_b, \dot{\boldsymbol{\eta}}_b, \mathbf{K}_o, \mathbf{D}_o). \quad (23b)$$

The following further assumption is considered.

• **Assumption 3.** The planned translational acceleration norm is bounded as

$$\|\ddot{\mathbf{p}}_d\| \leq \|\ddot{\mathbf{p}}_d\|_{max} = B_7. \quad (24)$$

Two main theorems will be employed in the following.

Theorem 1. Consider the generic perturbed system

$$\dot{\mathbf{x}} = \mathbf{f}(t, \mathbf{x}) + \mathbf{g}(t, \mathbf{x}). \quad (25)$$

Let $\mathbf{x} = \mathbf{0}$ be a globally exponentially stable equilibrium point of the nominal system

$$\dot{\mathbf{x}} = \mathbf{f}(t, \mathbf{x}). \quad (26)$$

Let $V(t, \mathbf{x})$ be a Lyapunov function of (26) satisfying the following inequalities

$$\gamma_1 \|\mathbf{x}\|^2 \leq V(t, \mathbf{x}) \leq \gamma_2 \|\mathbf{x}\|^2, \quad (27a)$$

$$\frac{\partial V}{\partial t} + \frac{\partial V}{\partial \mathbf{x}} \mathbf{f}(\mathbf{x}) \leq -\gamma_3 \|\mathbf{x}\|^2, \quad (27b)$$

$$\left\| \frac{\partial V}{\partial \mathbf{x}} \right\| \leq \gamma_4 \|\mathbf{x}\|, \quad (27c)$$

where $V(t, \mathbf{x})$ is defined in $[0, \infty) \times D = \{\|\mathbf{x}\| < \infty\}$ and $\gamma_i > 0$, with $i = 1, \dots, 4$. Suppose the perturbation term in (25) satisfies the uniform bound

$$\|\mathbf{g}(t, \mathbf{x})\| \leq \Delta < \infty, \quad (28)$$

for all $t \geq t_0$. Then, for all $\|\mathbf{x}(t_0)\| < \infty$, the solution $\mathbf{x}(t)$ of the perturbed system (25) satisfies

$$\|\mathbf{x}(t)\| \leq \xi e^{-\rho(t-t_0)} \|\mathbf{x}(t_0)\|, \quad \forall t_0 \leq t < t_i, \quad (29a)$$

$$\|\mathbf{x}(t)\| \leq B, \quad \forall t \geq t_i, \quad (29b)$$

for some finite time t_i , where

$$\xi = \sqrt{\frac{\gamma_2}{\gamma_1}}, \quad \rho = \frac{(1-\epsilon)\gamma_3}{2\gamma_2}, \quad B = \frac{\Delta\gamma_4}{\epsilon\gamma_3} \sqrt{\frac{\gamma_2}{\gamma_1}},$$

with $\epsilon < 1$.

Proof. See [55], Lemma 5.2. \square

Theorem 2. Consider a generic perturbed system like (25). Let $\mathbf{x} = \mathbf{0}$ be a globally exponentially stable equilibrium point of the nominal system (26). Let $V(t, \mathbf{x})$ be a Lyapunov function of (26) satisfying inequalities (27). Suppose the perturbation term in (25) satisfies the following inequality

$$\|\mathbf{g}(t, \mathbf{x})\| \leq \Gamma_1(t) \|\mathbf{x}\| + \Gamma_2(t), \quad (30)$$

where both $\Gamma_1(t)$ and $\Gamma_2(t)$ are nonnegative and continuous terms for all $t \geq t_0$. Moreover, $\Gamma_2(t)$ has to be also bounded for all $t \geq t_0$, while $\Gamma_1(t)$ must satisfy the following inequality

$$\int_{t_0}^t \Gamma_1(t) dt \leq b_1(t - t_0) + b_2, \quad (31)$$

for some nonnegative constants b_1 and b_2 , with

$$b_1 < \frac{\gamma_1 \gamma_3}{\gamma_2 \gamma_4}. \quad (32)$$

Then, for any initial condition of the state $\mathbf{x}(t_0)$, the solution of the perturbed system (25) satisfies the following bound

$$\|\mathbf{x}(t)\| \leq b_3, \quad (33)$$

with

$$b_3 = \max \left\{ \xi \frac{\gamma_2}{\gamma_1} \|\mathbf{x}(t_0)\|, \frac{\xi \gamma_4}{2\rho \gamma_2} b_4 \right\},$$

where

$$\xi = e^{\frac{\gamma_4 b_2}{2\gamma_1}},$$

$$\rho = \frac{1}{2} \left(\frac{\gamma_3}{\gamma_2} - b_1 \frac{\gamma_4}{\gamma_1} \right),$$

$$b_4 = \sup_{t \geq t_0} \Gamma_2(t).$$

Proof. See [55], Lemma 5.7. \square

By exploiting the two theorems introduced above, a two-steps procedure is employed to prove the stability of (22). First, the stability of (22b) is verified and the ultimate bound is found for the solution $\mathbf{x}_2(t)$, with $t \geq t_0$ and $t_0 \geq 0$ a generic starting time instant. Then, the stability of (22a) is verified considering also the interconnection with the angular closed-loop equation (22b) given by \mathbf{e}_η . However, before starting with these proofs, the boundedness of the errors of the momentum-based estimator is provided.

6.1. Boundedness of the external wrench and unmodeled dynamics estimation errors

A bound for the error of the momentum-based estimator of the external wrench and unmodeled dynamics is provided in this subsection. The detailed analysis is carried out for the estimated moments: a similar procedure is valid for the estimated forces.

Since $\tilde{\boldsymbol{\tau}} = \boldsymbol{\tau}_u - \hat{\boldsymbol{\tau}}_u$, the following equations hold

$$\dot{\tilde{\boldsymbol{\tau}}}_u = \boldsymbol{\tau}_u - \dot{\tilde{\boldsymbol{\tau}}}_u, \quad \dot{\hat{\boldsymbol{\tau}}}_u = \dot{\boldsymbol{\tau}}_u - \dot{\tilde{\boldsymbol{\tau}}}_u, \quad \ddot{\tilde{\boldsymbol{\tau}}}_u = \ddot{\boldsymbol{\tau}}_u - \ddot{\tilde{\boldsymbol{\tau}}}_u. \quad (34)$$

Equation (13) can be written in the following way for what concerns the moments' part

$$\ddot{\tilde{\boldsymbol{\tau}}}_u + \mathbf{K}_{1,2} \dot{\hat{\boldsymbol{\tau}}}_u + \mathbf{K}_{1,2} \mathbf{K}_{2,2} \hat{\boldsymbol{\tau}}_u = \mathbf{K}_{1,2} \mathbf{K}_{2,2} \boldsymbol{\tau}_u, \quad (35)$$

and substituting (34) into (35) yields

$$\ddot{\tilde{\boldsymbol{\tau}}} + \mathbf{K}_{1,2}\dot{\tilde{\boldsymbol{\tau}}} + \mathbf{K}_{1,2}\mathbf{K}_{2,2}\tilde{\boldsymbol{\tau}} = \ddot{\boldsymbol{\tau}}_u + \mathbf{K}_{1,2}\dot{\boldsymbol{\tau}}_u, \quad (36)$$

which is the considered perturbed systems representing the evolution of the error estimate of the unknown moments. The right side term in (36) denotes a disturbance against the convergence of the error estimate to zero. For sole constant unknown moments $\boldsymbol{\tau}_u$, the right side term in (36) vanishes, meaning a perfect estimate. Otherwise, due to delay introduced by the estimation dynamics in (13), the error remains anyway bounded as proven by the following corollary.

Corollary 1. *The error $\tilde{\boldsymbol{r}} = \begin{bmatrix} \tilde{\boldsymbol{\tau}}^T & \tilde{\boldsymbol{f}}^T \end{bmatrix}^T$ is bounded while estimating unknown perturbations satisfying (5). In particular, considering $\boldsymbol{x}_\tau = \begin{bmatrix} \tilde{\boldsymbol{\tau}}^T & \dot{\tilde{\boldsymbol{\tau}}}^T \end{bmatrix}^T$, the following ultimate bound holds*

$$\|\boldsymbol{x}_\tau(t)\| \leq \xi_1 e^{-\rho_1(t-t_0)} \|\boldsymbol{x}_\tau(t_0)\|, \quad \forall t_0 \leq t < t_1, \quad (37a)$$

$$\|\boldsymbol{x}_\tau(t)\| \leq B_8, \quad \forall t \geq t_1, \quad (37b)$$

for some positive constants ξ_1 , ρ_1 and B_8 defined in the proof. Moreover, in case of constant unknown forces \boldsymbol{f}_u and moments $\boldsymbol{\tau}_u$, the equilibrium points $\boldsymbol{x}_f = \begin{bmatrix} \tilde{\boldsymbol{f}}^T & \dot{\tilde{\boldsymbol{f}}}^T \end{bmatrix}^T = \mathbf{0}_6$ and $\boldsymbol{x}_\tau = \mathbf{0}_6$ are globally exponentially stable.

Proof. See Appendix A. \square

From (37) it is possible to have

$$\|\tilde{\boldsymbol{r}}\| \leq B_9 = \max\{\xi_1 \|\boldsymbol{x}_\tau(t_0)\|, B_8\}, \quad (38)$$

for all $t \geq t_0$, which represents the ultimate bound for the moments estimation error. Therefore, since the proof in Appendix A is performed for the estimated moments but the same procedure holds for the estimated forces, it is possible to conclude that

$$\|\tilde{\boldsymbol{f}}\| \leq B_{10}, \quad (39)$$

with $B_{10} > 0$ depending on B_2 and B_3 (see (5b)-(5c)).

- **Remark 5.** Taking into account the proof in Appendix A, if the unknown moments $\boldsymbol{\tau}_u$ are constants, the right side term in (36) vanishes. Hence $B_5 = B_6 = 0 \Rightarrow B_8 = \|\tilde{\boldsymbol{r}}\| = 0$, for all $t \geq t_1$.

6.2. Stability of the closed-loop equation (22b)

As shown by the following corollary, the closed-loop equation (22b) is stable for bounded perturbations and exponentially stable for constant unknown moments.

Corollary 2. *Under the given assumptions, considering the dynamic model of a generic VTOL UAV for the angular part (4b), the designed control law (15) and the compensation of the estimated moments in (12), the state error \boldsymbol{x}_2 , whose dynamics is given by the closed loop system (22b), is ultimately bounded as*

$$\|\boldsymbol{x}_2(t)\| \leq \xi_2 e^{-\rho_2(t-t_0)} \|\boldsymbol{x}_2(t_0)\|, \quad \forall t_0 \leq t < t_2, \quad (40a)$$

$$\|\boldsymbol{x}_2(t)\| \leq B_{11}, \quad \forall t \geq t_2, \quad (40b)$$

for some positive constants ξ_2 , ρ_2 and B_{11} defined in the proof. In particular, in case of constant unknown moments $\boldsymbol{\tau}_u$, the equilibrium point $\boldsymbol{x}_2 = \mathbf{0}_6$ is exponentially stable.

Proof. See Appendix B. \square

The following remark concludes the analysis.

- **Remark 6.** As underlined in Section 6.1, when only constant unknown moments $\boldsymbol{\tau}_u$ are present, the norm $\|\tilde{\boldsymbol{r}}\|$ goes asymptotically to zero. Hence, B_9 is zero as well as B_{11} for all $t \geq t_2$. Therefore, the closed-loop system (22b) becomes exponentially stable.

6.3. Stability of the closed-loop equation (22a)

As shown by the following corollary, the closed-loop equation (22a) is stable for bounded perturbations and exponentially stable for constant unknown moments and forces.

Corollary 3. *Under the given assumptions, considering the dynamic model of a generic VTOL UAV for the translational part (4a), the designed control law (19) and the compensation of the estimated unknown forces in (12), the state error \boldsymbol{x}_1 , whose dynamics is given by the closed loop system (22a), is ultimately bounded as*

$$\|\boldsymbol{x}_1(t)\| \leq B_{17}, \quad (41)$$

with B_{17} a finite positive bound given in the proof. In particular, in case of constant unknown forces \boldsymbol{f}_u and moments $\boldsymbol{\tau}_u$, the equilibrium point $\boldsymbol{x}_1 = \mathbf{0}_6$ is exponentially stable.

Proof. See Appendix C. \square

7. Experiments

7.1. Set-up and technical details

Experiments have been performed by using an Asctech Pelican quadrotor. Both the controller and the estimator have been implemented onboard at 100 Hz on an ATOM CPU with a patched RTAI real-time kernel UBUNTU OS. An OptiTrack motion-capture system has been employed to track both the position and translational velocity of the quadrotor. A ground station made up of a personal computer with UBUNTU OS is in charge of the WiFi communication between the OptiTrack system and the quadrotor as well as for the operator telemetry.

The mass m and the inertia \mathbf{I}_b of the vehicle that have been considered in the controller are 1.2 kg and $\text{diag}(3.4, 3.4, 4.7) \cdot 10^{-3} \text{ kgm}^2$, respectively. The vehicle parameters in (3) are $l = 0.21 \text{ m}$, $\rho_u = 1.8 \cdot 10^{-5} \text{ Ns}^2/\text{rad}^2$ and $c = 8 \cdot 10^{-7} \text{ Nms}^2/\text{rad}^2$.

Following Remark 2, the gains of the controller have been tuned as follows: $\mathbf{K}_p = \text{diag}(25, 25, 100)$, $\mathbf{D}_p = \text{diag}(10, 10, 20)$, for the translational part; $\mathbf{K}_o = \text{diag}(625, 625, 225)$, $\mathbf{D}_o = \text{diag}(50, 50, 30)$ for the angular part. The factor ν has been set to 100. Regarding the estimator, instead, the natural frequency and the damping factor have been tuned to 7 rad/s and 1, respectively, for all the force and moment components.

7.2. Case studies

Several case studies are considered in the following. The hovering and tracking performance of the passivity-based control are shown. It will be highlighted how the sole passivity-based control (see Remark 4) is able to perform all the tasks with a good accuracy, but that the compensation is crucial when unmodelled dynamics terms and unexpected situations become relevant. A video of the presented case studies and other different situations can be found in the multimedia attachment⁴.

7.2.1. Case study A

In this first case study, the quadrotor tracks three times a given circular trajectory with a constant speed of 0.5 m/s. The circle is planned in the x, y plane at a constant altitude of 1 m from the ground by choosing three different points. The resulting radius is about 0.83 m. After the take-off,

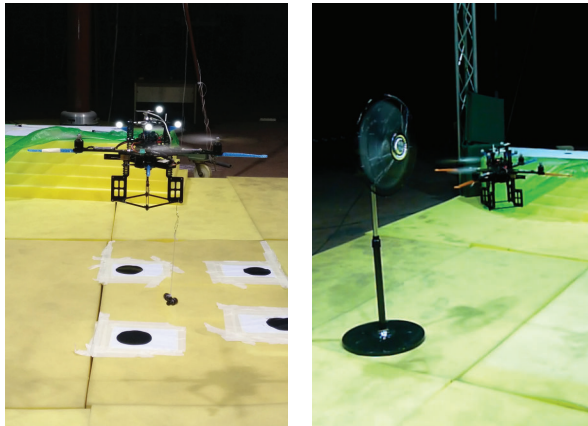


Figure 4: Left: quadrotor with the attached pendulum. Right: quadrotor in front of the fan.

the quadrotor reaches the first point of the circle and then executes the planned trajectory. At the end, the landing operation is commanded. In the following analysis represented in Fig. 3, the take-off, the landing and the first-point reaching phases are not shown.

The comparison between the norms of the position error in the case of the passivity-based control with and without the compensation of the external wrench and unmodeled dynamics is depicted in Fig. 3(a). The attitude error norms are instead shown in Fig. 3(b). It is possible to notice how the sole passivity-based control is able to successfully track the circle. The average position error norm is about 5 cm which could be acceptable in several practical tasks. However, the performance is substantially improved by using the information provided by the estimator of unknown forces and moments: the norm of the position error decreases to less than 2 cm. From Figs 3(e)-3(f) it is possible to notice that small uncertainties are present. For instance, the considered inertia \mathbf{I}_b might be inaccurate and the estimated force along the z axis might be an indicator about either a missing amount in the considered mass of the Pelican or that the commanded thrust is not perfectly equal to the actual one. The commanded propellers inputs in the two considered cases are represented in Figs 3(c)-3(d).

7.2.2. Case study B

In this second case study, the same circular trajectory of the previous situation is considered. However, an external load has been physically added and not considered in the controller. In par-

⁴Also available at: <http://youtu.be/iHKtHF0LF-w>

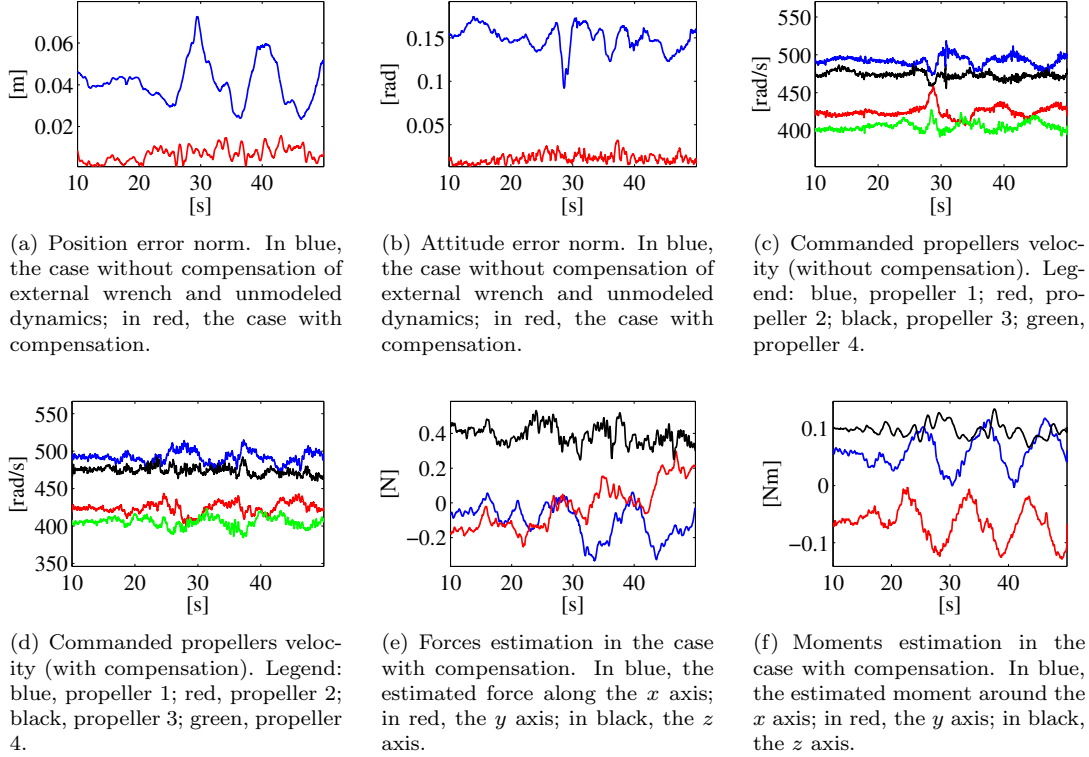


Figure 3: Case study A.

ticular, after the take-off, a pendulum has been attached, through a hook (see Fig. 4), to the bottom of the quadrotor and far from the vertical axis of the vehicle of about 15 cm. The pendulum has a mass of about 0.15 Kg and a length of 0.21 m.

The effect of the additional load is visible in Fig.s 5(e)-5(f), where now the estimated force reflects the presence of the additional mass of the pendulum. Moreover, comparing Fig. 3(f) with Fig. 5(f) it is possible to notice the effect of the oscillations of the pendulum during the circular trajectory resulting in the presence of significant unknown moments. These disturbances affect the performance of the controller. Namely, in the sole passivity-based control, the average position error norm is about 9 cm (see Fig. 5(a)), while the average attitude error norm is about 10 degrees (see Fig. 5(b)). However, in any case, such control exhibits robust properties in presence of unmodelled and unpredicted effects. The performance is increased by exploiting the compensation provided by the estimator as it is possible to see in Fig.s 5(a)-5(b). The commanded propellers inputs are represented in Fig.s 5(c)-5(d).

7.2.3. Case study C

In this last case study, the quadrotor is subject to an external disturbance caused by a fan (see Fig. 4). This fan is placed at about 1.1 m from the ground and at a distance of about 20 cm from the aerial vehicle in the x, y -plane. The quadrotor takes off at a height of about 0.6 m, then it reaches the altitude of 1.8 m passing in front of the fan. Then, it decreases again its altitude to 0.6 m (passing again through the wind flow generated by the fan) and finally goes in front of the fan at 1.1 m from the ground, simulating a persisting disturbance. After few seconds, the landing action is commanded. Each rectilinear path along the z axis is performed at a constant speed of 0.5 m/s. The take-off and the landing phases are neglected in the plots of Fig. 6.

Again, in general, by looking at Fig.s 6(a)-6(b), it is possible to notice that the sole passivity-based control is stable even in the presence of both time-varying and constant disturbances: the performance is poor and can be recovered exploiting the compensation provided by the estimator. Fig.s 6(e)-6(f) show the estimated forces and moments in the compensation case. It is possible to

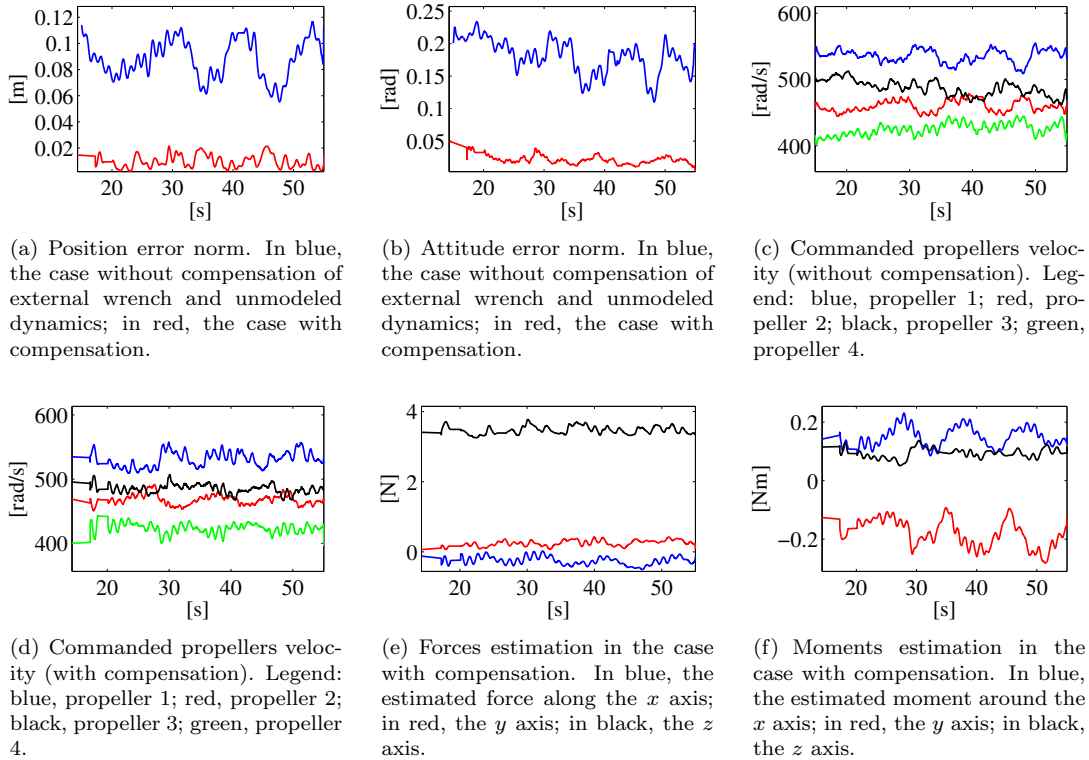


Figure 5: Case study B.

notice the first passage in front of the fan at about 20 s. Notice that the estimated forces are expressed with respect to Σ_i and the fan is aligned to the x axis of the inertial frame. The second passage in front of the fan is at about 25 s. Afterwards, the quadrotor stays in front of the fan from the time instant at 31 s until the landing command is given. At that point, it is possible to notice that the estimated forces are almost constant (about 0.8 N along the x axis), while the estimated moments wave due to small oscillations of the aerial platform caused by small turbulent aerodynamic effects on the UAV. This last causes also a small estimated force along z axis. The commanded propellers inputs are represented in Fig.s 6(c)-6(d).

8. Conclusion and future work

A momentum-based estimator of external wrench and unmodeled dynamics has been employed in this paper to control a VTOL UAV together with a passivity-based control. The algorithm enables to successfully perform hovering and tracking tasks with a good accuracy. The robustness of the control

has been tested in presence of unmodelled dynamic parameters and external disturbances. However, even if the stability of the controller is preserved, the performance might be poor in this last case. For this reason, the presence of an estimator of forces and moments becomes crucial in presence of uncertainties. Compensation of such terms results in a stable controller with good performance in several different unexpected conditions and situations. Under certain assumptions, theoretical results prove the stability of the closed-loop systems including the proposed estimator. Experiments have been performed to illustrate the performance of the proposed control in real tasks.

Future work will be focused on problems related to outdoor scenarios: in particular, the effects on introducing an estimated translational velocity rather than using the one provided by a visual tracker. Moreover, the proposed architecture will be tested in a real aerial manipulation task.

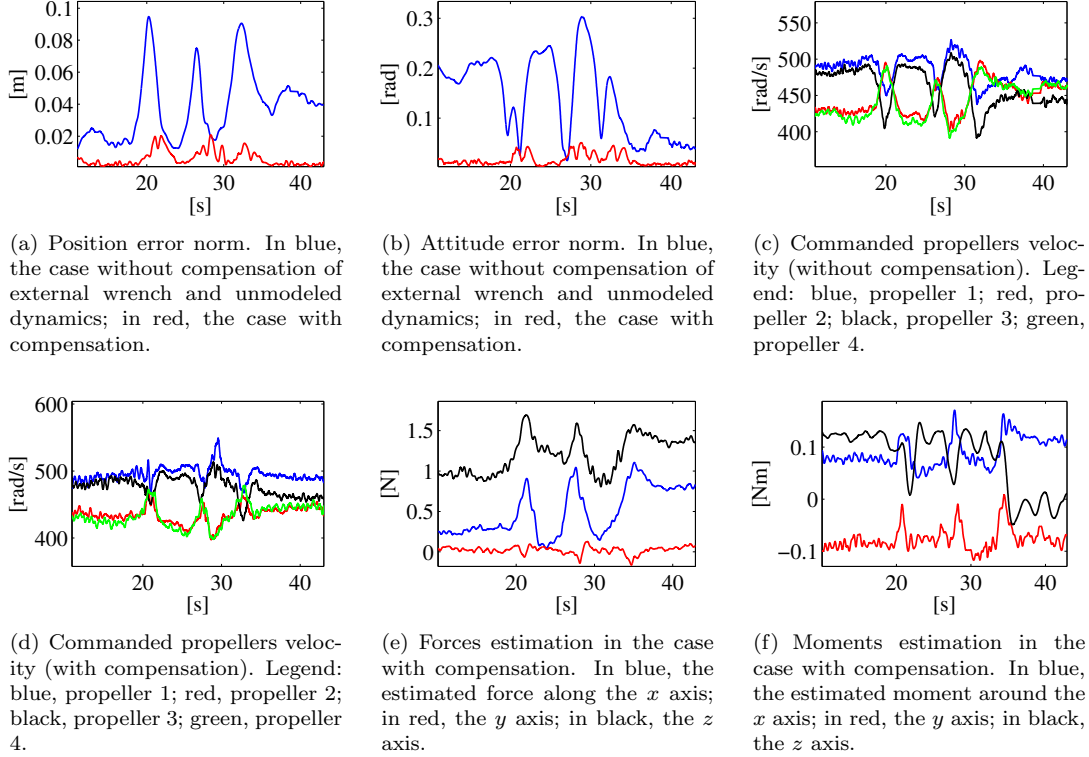


Figure 6: Case study C.

Acknowledgements

The research leading to these results has been supported by the ARCAS and SHERPA collaborative projects, which both have received funding from the European Community Seventh Framework Programme (FP7/2007-2013) under grant agreements ICT-287617 and ICT-600958, respectively. The authors are solely responsible for its content. It does not represent the opinion of the European Community and the Community is not responsible for any use that might be made of the information contained therein.

Appendix A. Proof of Corollary 1

Proof. Considering Theorem 1, the nominal system associated to (36) is

$$\alpha_\tau(\mathbf{x}_\tau) = \ddot{\tilde{\boldsymbol{\tau}}} + \mathbf{K}_{1,2}\dot{\tilde{\boldsymbol{\tau}}} + \mathbf{K}_{1,2}\mathbf{K}_{2,2}\tilde{\boldsymbol{\tau}} = \mathbf{0}_6. \quad (\text{A.1})$$

The origin $\mathbf{x}_\tau = \mathbf{0}_6$ of the linear system (A.1) is globally exponentially stable since (A.1) is a second-order differential linear equation with $\mathbf{K}_{1,2}$ and

$\mathbf{K}_{2,2}$ positive definite matrices. Therefore, the following function

$$V_1(\mathbf{x}_\tau) = \frac{1}{2}\mathbf{x}_\tau^T \mathbf{P}_1 \mathbf{x}_\tau, \quad (\text{A.2})$$

is a Lyapunov function for (A.1), in which \mathbf{P}_1 is a (6×6) positive definite symmetric matrix solving the following equation

$$\mathbf{P}_1 \mathbf{A}_1 + \mathbf{A}_1^T \mathbf{P}_1 + \mathbf{\Lambda}_1 = \mathbf{O}_6, \quad (\text{A.3})$$

for any (6×6) definite positive symmetric matrix $\mathbf{\Lambda}_1$, with \mathbf{A}_1 the linear matrix associated to (A.1), depending on $\mathbf{K}_{1,2}$ and $\mathbf{K}_{2,2}$. Through this choice of $V_1(\mathbf{x}_\tau)$, the bounds in (27) are verified as follows [55]

$$\gamma_1 = \underline{\lambda}_{P_1}, \quad \gamma_2 = \bar{\lambda}_{P_1}, \quad \gamma_3 = \underline{\lambda}_{\Lambda_1}, \quad \gamma_4 = 2\bar{\lambda}_{P_1}, \quad (\text{A.4})$$

where $\bar{\lambda}$ and $\underline{\lambda}$ are the maximum and minimum eigenvalues, respectively, of the associated matrix.

Taking into account (5e) and (5f), the bound in (28) of the perturbation term $\dot{\tilde{\boldsymbol{\tau}}}_u + \mathbf{K}_{1,2}\tilde{\boldsymbol{\tau}}_u$ is satisfied with

$$\Delta = \bar{\lambda}_{K_{1,2}} B_5 + B_6, \quad (\text{A.5})$$

for all $t \geq t_0$.

Then, considering (29), for all $\|\mathbf{x}_\tau(t_0)\| < \infty$, the solution $\mathbf{x}_\tau(t)$ of the perturbed system (36) satisfies (37) for some finite time t_1 , depending on (A.5) and $\|\mathbf{x}_\tau(t_0)\|$, where

$$\xi_1 = \sqrt{\frac{\bar{\lambda}_{P_1}}{\underline{\lambda}_{P_1}}}, \quad \rho_1 = \frac{(1 - \epsilon_1)\underline{\lambda}_{\Lambda_1}}{2\bar{\lambda}_{P_1}},$$

with $\epsilon_1 < 1$ and

$$B_8 = \frac{2\bar{\lambda}_{P_1}(\bar{\lambda}_{K_{1,2}}B_5 + B_6)}{\epsilon_1\underline{\lambda}_{\Lambda_1}} \sqrt{\frac{\bar{\lambda}_{P_1}}{\underline{\lambda}_{P_1}}}. \quad (\text{A.6})$$

The same procedure can be applied for the estimated forces. \square

It is worth noticing that B_8 can be decreased through a proper choice of the gains $\mathbf{K}_{1,2}$ and $\mathbf{K}_{2,2}$ and of the matrix $\mathbf{\Lambda}_1$.

Appendix B. Proof of Corollary 2

Proof. Theorem 1 is taken into account for the demonstration. In order to show that $\mathbf{x}_2 = \mathbf{0}_6$ is a globally exponentially stable equilibrium point of the nominal closed-loop equation (23b), the inequalities in (27) have to be satisfied [55]. Therefore, consider the following candidate Lyapunov function inspired by [53]

$$V_2(t, \mathbf{x}_2) = \frac{1}{2} \mathbf{x}_2^T \mathbf{P}_2 \mathbf{x}_2, \quad (\text{B.1})$$

with

$$\mathbf{P}_2 = \begin{bmatrix} \mathbf{K}_o + 2\nu\mathbf{D}_o + \nu^2\mathbf{M}(\boldsymbol{\eta}_b) & \nu\mathbf{M}(\boldsymbol{\eta}_b) \\ \nu\mathbf{M}(\boldsymbol{\eta}_b) & \mathbf{M}(\boldsymbol{\eta}_b) \end{bmatrix}.$$

Thanks to Sylvester's criterion, it is possible to verify that the quadratic form in (B.1) is positive definite and vanishes only when $\mathbf{x}_2 = \mathbf{0}_6$. Inequality (27a) is then proved with $\gamma_1 = \frac{1}{2}\underline{\lambda}_{P_2}$ and $\gamma_2 = \frac{1}{2}\bar{\lambda}_{P_2}$. In order to verify (27b), the following inequality holds

$$\frac{\partial V_2}{\partial t} + \frac{\partial V_2}{\partial \mathbf{x}_2} \boldsymbol{\alpha}_2(\nu, \mathbf{x}_2, \boldsymbol{\eta}_b, \dot{\boldsymbol{\eta}}_b, \mathbf{K}_o, \mathbf{D}_o) \leq -\mathbf{x}_2^T \mathbf{\Lambda}_2 \mathbf{x}_2,$$

with

$$\mathbf{\Lambda}_2 = \begin{bmatrix} \nu\mathbf{K}_o + \nu^2\mathbf{D}_o & \mathbf{O}_3 \\ \mathbf{O}_3 & \mathbf{D}_o \end{bmatrix}.$$

It is possible to easily check that $\mathbf{\Lambda}_2$ is positive definite and then (27b) is verified through $\gamma_3 = \underline{\lambda}_{\Lambda_2}$. Finally, inequality (27c) is proved with $\gamma_4 = \bar{\lambda}_{P_2}$.

Taking into account (38), the uniform bound in (28) is proved as follows

$$\|\boldsymbol{\beta}_2(\boldsymbol{\eta}_b, \tilde{\boldsymbol{\tau}})\| \leq \bar{\lambda}_{M^{-1}} \|\tilde{\boldsymbol{\tau}}\| \leq \bar{\lambda}_{M^{-1}} B_9 < \infty. \quad (\text{B.2})$$

Then, considering (29), for all $\|\mathbf{x}_2(t_0)\| < \infty$, the solution $\mathbf{x}_2(t)$ of the perturbed system (22b) satisfies (40) for some finite amount of time $t_2 \geq t_1$, depending on (B.2) and $\|\mathbf{x}_2(t_0)\|$, where

$$\xi_2 = \sqrt{\frac{\bar{\lambda}_{P_2}}{\underline{\lambda}_{P_2}}}, \quad \rho_2 = \frac{(1 - \epsilon_2)\underline{\lambda}_{\Lambda_2}}{\bar{\lambda}_{P_2}},$$

with $\epsilon_2 < 1$ and

$$B_{11} = \frac{\bar{\lambda}_{P_2} \bar{\lambda}_{M^{-1}} B_9}{\epsilon_2 \underline{\lambda}_{\Lambda_2}} \sqrt{\frac{\bar{\lambda}_{P_2}}{\underline{\lambda}_{P_2}}}. \quad (\text{B.3})$$

\square

The following two remarks conclude the proof.

- **Remark 7.** As highlighted in Remark 4, it is not ensured in principle that the compensation of estimated generalized forces improves the performance of the sole passivity-based controller. In order to check whether the compensation is convenient or not, the case where the estimations are not employed is considered. In such a case, the perturbation term in (22b) appears to be

$$\boldsymbol{\beta}'_2(\boldsymbol{\eta}_b, \boldsymbol{\tau}_u) = \begin{bmatrix} \mathbf{0}_3 \\ \mathbf{M}(\boldsymbol{\eta}_b)^{-1} \boldsymbol{\tau}_u \end{bmatrix}.$$

Corollary 2 still holds, but now inequality (B.2), which is necessary to prove hypothesis (28), is modified as follows

$$\|\boldsymbol{\beta}'_2(\boldsymbol{\eta}_b)\| \leq \bar{\lambda}_{M^{-1}} \|\boldsymbol{\tau}_u\| \leq \bar{\lambda}_{M^{-1}} B_4 = \Delta' < \infty,$$

where (5d) has been taken into account. On the one hand, in case only constant unknown moments $\boldsymbol{\tau}_u$ are present, estimated, and compensated, Δ' is always greater than 0, since $B_4 > 0$, while B_9 in (B.2) is zero from Remark 6. Hence, $B'_{11} > B_{11} = 0$: the bound with the compensation is less than the case without the compensation meaning that the performance of the controller is improved when a feedback of the unknown moments estimation is provided in (15). On the other hand, when time-varying unknown moments $\boldsymbol{\tau}_u$ are present, estimated, and compensated, $B_{11} <$

$B'_{11} \iff \bar{\lambda}_{M^{-1}} B_9 < \Delta'$, meaning that compensation of the estimated moments is convenient in (15) when $B_9 < B_4$. This is in general verified when τ_u is slow-time varying and thanks to a proper choice of both estimator bandwidth and matrix Λ_1 in (A.3).

- **Remark 8.** Notice that inequality (40b) might be used to verify that the controller maintains the selected Euler angles in a singularity-free zone (see Assumption 1). Nevertheless, the mathematical derivation is cumbersome due to the complicated expression of B_{11} in (B.3). Experiments performed in Section 7 seem anyway very promising from this point of view.

Appendix C. Proof of Corollary 3

Proof. Theorem 2 is taken into account for the demonstration. The nominal closed-loop system (23a) has a unique exponentially equilibrium point $\mathbf{x}_1 = \mathbf{0}_6$, since (23a) is a linear system with an associated (6×6) state matrix $\mathbf{A}_2(\mathbf{x}_1)$ which is Hurwitz, since $m > 0$ and both \mathbf{K}_p and \mathbf{D}_p are positive definite diagonal matrices. Therefore, the following function

$$V_3(\mathbf{x}_1) = \frac{1}{2} \mathbf{x}_1^T \mathbf{P}_3 \mathbf{x}_1, \quad (\text{C.1})$$

is a Lyapunov function for (23a), in which \mathbf{P}_3 is a (6×6) positive definite symmetric matrix solving the following equation

$$\mathbf{P}_3 \mathbf{A}_2 + \mathbf{A}_2^T \mathbf{P}_3 + \Lambda_3 = \mathbf{O}_6, \quad (\text{C.2})$$

for any (6×6) definite positive symmetric matrix Λ_3 . Through this choice of $V_3(\mathbf{x}_1)$, inequalities (27) are verified with the following choice of the bounds [55]

$$\gamma_1 = \underline{\lambda}_{P_3}, \quad \gamma_2 = \bar{\lambda}_{P_3}, \quad \gamma_3 = \underline{\lambda}_{\Lambda_3}, \quad \gamma_4 = 2\bar{\lambda}_{P_3}. \quad (\text{C.3})$$

Taking into account (5a), (16), (19), (24), (39) and the equation $\hat{\mathbf{f}}_u = \mathbf{f}_u - \tilde{\mathbf{f}}$, it is possible to give the following ultimate bound to the thrust

$$\begin{aligned} |u| &= m \|\ddot{\mathbf{p}}_d - \mathbf{g} - \frac{1}{m} \mathbf{D}_p \dot{\mathbf{e}}_p - \frac{1}{m} \mathbf{K}_p \mathbf{e}_p - \frac{1}{m} \hat{\mathbf{f}}_u\| \\ &\leq B_{12} + B_{13} (\|\mathbf{e}_p\| + \|\dot{\mathbf{e}}_p\|) \\ &\leq B_{12} + B_{13} \sqrt{2} \|\mathbf{x}_1\|, \end{aligned} \quad (\text{C.4})$$

where $B_{12} = B_1 + m(g + B_7) + B_{10}$ and $B_{13} = \max\{\bar{\lambda}_{K_p}, \bar{\lambda}_{D_p}\}$. The ultimate bound for the term $\delta(\boldsymbol{\eta}_d, \mathbf{e}_\eta)$ in $\beta_1(u, m, \boldsymbol{\eta}_d, \mathbf{e}_\eta, \tilde{\mathbf{f}})$ is

$$\|\delta(\boldsymbol{\eta}_d, \mathbf{e}_\eta)\| \leq B_{14} \|\mathbf{e}_\eta\|, \quad (\text{C.5})$$

with $B_{14} > 0$. By recalling (18) and exploiting the following general relationships

$$\begin{aligned} \sin(a+b) &= \sin(a) + 2 \sin(b/2) \cos(a+b/2) \\ \cos(a+b) &= \cos(a) - 2 \sin(b/2) \sin(a+b/2) \\ |\sin(a)| &\leq |a|, \quad |\sin(a)| \leq 1, \quad |\cos(a)| \leq 1 \\ \prod_{i=1}^n |a_i| &\leq \frac{1}{2} \sum_{i=1}^n |a_i|, \quad \text{for } |a_i| \leq 1, \end{aligned}$$

inequality (C.5) can be verified providing first a bound to $|\delta_x|$, $|\delta_y|$ and $|\delta_z|$ and then considering $\|\delta(\boldsymbol{\eta}_d, \mathbf{e}_\eta)\| = \sqrt{\delta_x^2 + \delta_y^2 + \delta_z^2}$. Notice that $|\sin(a)| \leq |a|$ and $|\sin(a)| \leq 1$ are employed with arguments e_Υ and $e_\Upsilon + \Upsilon_d$, respectively, with $\Upsilon = \{\phi, \theta, \psi\}$. Hence, taking into account (39), (C.4) and (C.5), the following ultimate bound can be written for the perturbation term $\beta_1(u, m, \boldsymbol{\eta}_d, \mathbf{e}_\eta, \tilde{\mathbf{f}})$

$$\|\beta_1\| \leq \frac{1}{m} (B_{10} + B_{13} B_{14} \sqrt{2} \|\mathbf{e}_\eta\| \|\mathbf{x}_1\| + B_{12} B_{14} \|\mathbf{e}_\eta\|). \quad (\text{C.6})$$

Comparing (30) and (C.6), it is possible to recognize that $\Gamma_1(t) = (B_{13} B_{14} \sqrt{2} / m) \|\mathbf{e}_\eta\|$, while $\Gamma_2(t) = (1/m) (B_{10} + B_{12} B_{14} \|\mathbf{e}_\eta\|)$. Notice that both $\Gamma_1(t)$ and $\Gamma_2(t)$ are nonnegative and continuous terms for all $t \geq t_0$. Moreover, $\Gamma_2(t)$ is bounded for all $t \geq t_0$ since

$$\Gamma_2(t) = \frac{B_{10} + B_{12} B_{14} \|\mathbf{e}_\eta\|}{m} \leq \frac{B_{10} + B_{12} B_{14} B_{15}}{m},$$

in which (40) has been considered, with $B_{15} = \max\{\xi_2 \|\mathbf{x}_2(t_0)\|, B_{11}\}$. In order to verify (31), denoting with $Y = (B_{13} B_{14} / m) \sqrt{2}$, the following inequality holds for $\Gamma_1(t)$

$$\begin{aligned} Y \int_{t_0}^t \|\mathbf{e}_\eta\| dt &= Y \left(\int_{t_0}^{t_2} \|\mathbf{e}_\eta\| dt + \int_{t_2}^t \|\mathbf{e}_\eta\| dt \right) \\ &\leq Y (\xi_2 B_{16} \|\mathbf{e}_\eta(t_0)\| + B_{11} (t - t_2)) \\ &< Y (\xi_2 B_{16} \|\mathbf{e}_\eta(t_0)\| + B_{11} (t - t_0)) \end{aligned} \quad (\text{C.7})$$

where $B_{16} = (1/\rho_2) e^{\rho_2 t_0} (e^{-\rho_2 t_0} - e^{-\rho_2 t_2})$. Hence, inequality (31) is verified with $b_1 = Y B_{11} > 0$ and $b_2 = Y B_{16} \xi_2 \|\mathbf{e}_\eta(t_0)\|$. Notice that b_2 is always

positive and bounded. Therefore, taking into account (31) and (C.7), fixing the desired gains \mathbf{K}_p and \mathbf{D}_p , noticing the dependency from the mass of the vehicle m and the bound B_{11} , it is then always possible to choose a matrix $\mathbf{\Lambda}_3$ such that inequality (32) is verified.

Then, considering (33), for any initial condition of the state $\mathbf{x}_1(t_0)$, the solution of the closed-loop system (22a) satisfies (41) with

$$B_{17} = \max \left\{ \xi_3 \frac{\bar{\lambda}_{P_3}}{\underline{\lambda}_{P_3}} \|\mathbf{x}_1(t_0)\|, \frac{\xi_3 \bar{\lambda}_{P_3}}{\rho_3 \bar{\lambda}_{P_3}} B_{18} \right\},$$

where

$$\xi_3 = e^{\frac{-Y \bar{\lambda}_{P_3} - B_{16} \xi_2 \|\mathbf{e}_\eta(t_0)\|}{\underline{\lambda}_{P_3}}},$$

$$\rho_3 = \frac{1}{2} \left(\frac{\underline{\lambda}_{\Lambda_3}}{\bar{\lambda}_{P_3}} - 2Y B_{11} \frac{\bar{\lambda}_{P_3}}{\underline{\lambda}_{P_3}} \right),$$

$$B_{18} = \sup_{t \geq t_0} \Gamma_2(t).$$

□

The following remark concludes the analysis.

- **Remark 9.** Notice that if only constant unknown moments $\boldsymbol{\tau}_u$ are present, estimated, and compensated, then B_{11} is zero from Remark 6. As a consequence, $b_1 = 0$ for all $t \geq t_2$. Inequality (32) is thus verified for any value of $\mathbf{\Lambda}_3$, \mathbf{K}_p and \mathbf{D}_p , while $\mathbf{x}_1(t)$'s bound in (41) depends only on B_{10} , which is due to the force estimation process. Therefore, if only constant unknown forces \mathbf{f}_u are present, estimated, and compensated, then $B_{10} = 0$ thanks to a similar consideration as in Remark 6, and $\mathbf{x}_1(t)$ goes asymptotically to zero. Furthermore, similar considerations can be done as in Remark 7 to show that compensation of estimated forces is convenient.

References

- [1] V. Lippiello, B. Siciliano, Wall inspection control of a VTOL unmanned aerial vehicle based on a stereo optical flow, in: 2012 IEEE/RSJ International Conference on Intelligent Robots and Systems, Vilamoura, P, 2012, pp. 4296–4302.
- [2] L. Marconi, F. Basile, G. Caprari, R. Carloni, P. Chiacchio, C. Huerzeler, V. Lippiello, R. Naldi, N. Janosch, B. Siciliano, S. Stramigioli, E. Zwicker, Aerial service robotics: The AIRobots perspective, in: 2nd International Conference on Applied Robotics for the Power Industry, Zurich, CH, 2012.
- [3] P. Oh, W. Green, CQAR: Closed Quarter Aerial Robot design for reconnaissance, surveillance and target acquisition tasks in urban areas, *International Journal of Computational Intelligence* 1 (4) (2004) 353–360.
- [4] P. Pounds, D. Bersak, A. Dollar, Grasping from the air: Hovering capture and load stability, in: 2011 IEEE International Conference on Robotics and Automation, Shanghai, CN, 2011, pp. 2491–2498.
- [5] G. Arleo, F. Caccavale, G. Muscio, F. Pierri, Control of quadrotor aerial vehicles equipped with a robotic arm, in: 21st Mediterranean Conference on Control and Automation, Crete, GR, 2013.
- [6] F. Forte, R. Naldi, A. Macchelli, L. Marconi, Impedance control of an aerial manipulator, in: Proceedings of 2012 American Control Conference, Montreal, CDN, 2012, pp. 3839–3844.
- [7] C. Korpela, M. Orsag, P. Oh, Hardware-in-the-loop verification for mobile manipulating unmanned aerial vehicles, *Journal of Intelligent and Robotic Systems* 73 (1–4) (2014) 725–736.
- [8] C. Korpela, M. Orsag, P. Oh, Towards valve turning using a dual-arm aerial manipulator, in: 2014 IEEE/RSJ International Conference on Intelligent Robots and Systems, Chicago, IL, USA, 2014, pp. 3411–3416.
- [9] V. Lippiello, F. Ruggiero, Exploiting redundancy in Cartesian impedance control of UAVs equipped with a robotic arm, in: 2012 IEEE/RSJ International Conference on Intelligent Robots and Systems, Vilamoura, P, 2012, pp. 3768–3773.
- [10] V. Lippiello, F. Ruggiero, Cartesian impedance control of a UAV with a robotic arm, in: 10th International IFAC Symposium on Robot Control, Dubrovnik, HR, 2012, pp. 704–709.
- [11] I. Maza, J. Kondak, M. Bernard, A. Ollero, Multi-UAV cooperation and control for load transportation and deployment, *Journal of Intelligent and Robotics Systems* 57 (1) (2010) 417–449.
- [12] R. Mebarki, V. Lippiello, B. Siciliano, Exploiting image moments for aerial manipulation control, in: ASME Dynamic Systems and Control Conference, Palo Alto, CA, 2013.
- [13] M. Orsag, C. Korpela, P. Oh, Modeling and control of MM-UAV: Mobile manipulating unmanned aerial vehicle, *Journal of Intelligent and Robotic Systems* 69 (1–4) (2013) 227–240.
- [14] I. Palunko, P. Cruz, R. Fierro, Agile load transportation. Safe and efficient load manipulation with aerial robots, *Robotics and Automation Magazine* 19 (3) (2012) 69–79.
- [15] K. Suseong, C. Seungwon, H. Kim, Aerial manipulation using a quadrotor with a two DOF robotic arm, in: 2013 IEEE International Conference On Intelligent Robots and Systems, Tokyo, J, 2013, pp. 4990–4995.
- [16] H. Yang, D. Lee, Dynamics and control of quadrotor with robotic manipulator, in: 2014 IEEE International Conference on Robotics and Automation, Hong Kong, C, 2014, pp. 5544–5549.
- [17] K. Nonami, F. Kendoul, S. Suzuki, W. Wang, *Autonomous Flying Robots. Unmanned Aerial Vehicles and Micro Aerial Vehicles*, Springer-Verlag, Berlin Heidelberg, D, 2010.
- [18] A. De Luca, A. Albu-Schaffer, S. Haddadin, G. Hirzinger, Collision detection and safe reaction with the DLR-III lightweight manipulator arm, in: IEEE/RSJ International Conference on Intelligent

- Robots and Systems, Beijing, C, 2006, pp. 1623–1630.
- [19] M. Kobilarov, Nonlinear trajectory control of multi-body aerial manipulators, *Journal of Intelligent and Robotic Systems* 73 (1–4) (2014) 679–692.
- [20] F. Ruggiero, M. Trujillo, R. Cano, H. Ascorbe, A. Viguria, C. Pérez, V. Lippiello, A. Ollero, B. Siciliano, A multilayer control for multirotor UAVs equipped with a servo robot arm, in: 2015 IEEE International Conference on Robotics and Automation, Seattle, WA, USA, 2015, (accepted for publication).
- [21] R. Mahony, T. Hamel, Robust trajectory tracking for a scale model autonomous helicopter, *International Journal of Robust and Nonlinear Control* 14 (12) (2004) 1035–1059.
- [22] T. Madani, A. Benallegue, Backstepping control for a quadrotor helicopter, in: IEEE/RSJ International Conference on Intelligent Robots and Systems, Beijing, C, 2006, pp. 3255–3260.
- [23] M. Fumagalli, R. Carloni, A modified impedance control for physical interaction of UAVs, in: 2013 IEEE/RSJ International Conference on Intelligent Robots and Systems, Tokyo, J, 2013, pp. 1979–1984.
- [24] V. Lippiello, G. Loianno, B. Siciliano, MAV indoor navigation based on a closed-form solution for absolute scale velocity estimation using optical flow and inertial data, in: 50th IEEE Conference on Decision Control and European Control Conference, Orlando, FL, 2011, pp. 3566–3571.
- [25] A. Roberts, A. Tayebi, Adaptive position tracking of VTOL UAVs, *IEEE Transactions on Robotics* 27 (1) (2011) 129–142.
- [26] G. Antonelli, F. Arrichiello, S. Chiaverini, P. Robuffo Giordano, Adaptive trajectory tracking for quadrotor MAVs in presence of parameter uncertainties and external disturbances, in: Proceedings 2013 IEEE/ASME International Conference on Advanced Intelligent Mechatronic, Wollongong, AU, 2013, pp. 1337–1342.
- [27] G. Antonelli, E. Cataldi, P. Robuffo Giordano, S. Chiaverini, A. Franchi, Experimental validation of a new adaptive control scheme for quadrotors MAVs, in: 2013 IEEE/RSJ International Conference on Intelligent Robots and Systems, Tokyo, J, 2013, pp. 3496–3501.
- [28] Z. Dydek, A. Annaswamy, E. Lavretsky, Adaptive control of quadrotor UAVs: A design trade study with flight evaluations, *IEEE Transactions on Control Systems Technology* 21 (4) (2013) 1400–1406.
- [29] D. Cabecinhas, R. Cunha, C. Silvestre, A nonlinear quadrotor trajectory tracking controller with disturbance rejection, *Control Engineering Practice* 26 (2014) 1–10.
- [30] B. Yüksel, C. Secchi, H. Bühlhoff, A. Franchi, A nonlinear force observer for quadrotors and application to physical interactive tasks, in: 2014 IEEE/ASME International Conference on Advanced Intelligent Mechatronics, Besançon, F, 2014, pp. 433–440.
- [31] T. Madani, A. Benallegue, Sliding mode observer and backstepping control for a quadrotor unmanned aerial vehicles, in: Proceedings of the 2007 American Control Conference, New York City, NY, 2007, pp. 5887–5892.
- [32] R. Mahony, S. Stramigioli, J. Trumpf, Vision based control of aerial robotic vehicles using the port Hamiltonian framework, in: 50th IEEE Conference on Decision Control and European Control Conference, Orlando, FL, 2011, pp. 3526–3532.
- [33] B. Yüksel, C. Secchi, H. Bühlhoff, A. Franchi, Reshaping the physical properties of a quadrotor through IDA-PBC and its application to aerial physical interaction, in: 2014 IEEE International Conference on Robotics and Automation, Honk Kong, C, 2014, pp. 6258–6265.
- [34] C. Ha, Z. Zuo, F. Choi, D. Lee, Passivity-based adaptive backstepping control of quadrotor-type UAVs, *Robotics and Autonomous Systems* 62 (9) (2014) 1305–1315.
- [35] O. Egeland, J.-M. Godhavn, Passivity-based adaptive attitude control of a rigid spacecraft, *IEEE Transactions on Automatic Control* 39 (4) (1994) 842–846.
- [36] S. Formentin, M. Lovera, Flatness-based control of a quadrotor helicopter via feedforward linearization, in: 2011 50th IEEE International Conference on Decision and Control and European Control Conference, Orlando, FL, USA, 2011, pp. 6171–6176.
- [37] F. Lizarralde, J. T. Wen, Attitude control without angular velocity measurement: A passivity approach, *IEEE Transactions on Automatic Control* 41 (3) (1996) 468–472.
- [38] P. Tsiotras, Further passivity results for the attitude control problem, *IEEE Transactions on Automatic Control* 43 (11) (1998) 1597–1600.
- [39] J. Slotine, W. Li, On the adaptive control of robot manipulators, *International Journal of Robotics Research* 6 (3) (1987) 49–59.
- [40] H. Berghuis, H. Nijmeijer, A passivity approach to controller-observer design for robots, *IEEE Transactions on Robotics and Automation* 9 (6) (1993) 740–754.
- [41] F. Ruggiero, J. Cacace, H. Sadeghian, V. Lippiello, Impedance control of VTOL UAVs with a momentum-based external generalized forces estimator, in: 2014 IEEE International Conference on Robotics and Automation, Hong Kong, C, 2014, pp. 2093–2099.
- [42] B. Siciliano, L. Sciavicco, L. Villani, G. Oriolo, *Robotics: Modelling, Planning and Control*, Springer, London, UK, 2008.
- [43] M.-D. Hua, T. Hamel, P. Morin, C. Samson, A control approach for thrust-propelled underactuated vehicles and its application to VTOL drones, *IEEE Transactions on Automatic Control* 54 (8) (2009) 1837–1853.
- [44] S. Omari, M.-D. Hua, G. Ducard, T. Hamel, Nonlinear control of VTOL UAVs incorporating flapping dynamics, in: 2013 IEEE/RSJ International Conference on Intelligent Robots and Systems, Tokyo, J, 2013, pp. 2419–2425.
- [45] J.-Y. Wen, K. Kreutz-Delgado, The attitude control problem, *IEEE Transactions on Automatic Control* 36 (10) (1991) 1148–1162.
- [46] A. Tayebi, S. McGilvray, Attitude stabilization of a VTOL quadrotor aircraft, *IEEE Transactions on Control Systems Technology* 14 (3) (2006) 562–571.
- [47] A. Tayebi, Unit quaternion-based output feedback for the attitude tracking problem, *IEEE Transactions on Automatic Control* 52 (6) (2008) 1516–1520.
- [48] C. Mayhew, R. Sanfelice, A. Teel, On quaternion-based attitude control and the unwinding phenomenon, in: 2011 American Control Conference, San Francisco, CA, USA, 2011, pp. 299–304.
- [49] R. Mebarki, J. Cacace, V. Lippiello, Velocity estimation of an UAV using visual and IMU data in a GPS-denied environment, in: 11th IEEE International Symposium on Safety, Security, and Rescue Robotics, Linköping, S,

- 2013.
- [50] R. Mebarki, V. Lippiello, Image moments-based velocity estimation of UAVs in GPS denied environments, in: 12th IEEE International Symposium on Safety, Security, and Rescue Robotics, Toyako-cho, Hokkaido, J, 2014.
 - [51] P. Fliess, J. Levine, P. Rouchon, Flatness and defect of nonlinear systems: Introductory theory and examples, *International Journal of Control* 61 (6) (1995) 1327–1361.
 - [52] C. Ott, Cartesian Impedance Control of Redundant and Flexible-Joint Robots, Vol. 49 of Springer Tracts in Advanced Robotics, Springer-Verlag, Berlin Heidelberg, D, 2008.
 - [53] W. Chung, L.-C. Fu, S.-H. Hsu, Motion control, in: B. Siciliano, O. Khatib (Eds.), *Springer Handbook of Robotics*, Springer, 2008, pp. 133–159.
 - [54] G. Antonelli, On the use of adaptive/integral actions for 6-degrees-of-freedom control of autonomous underwater vehicles, *IEEE Journal of Oceanic Engineering* 32 (2) (2007) 300–312.
 - [55] H. Khalil, *Nonlinear systems*, Prentice Hall, Upper Saddle River, NJ, 2002.